ExoPlex: A New Python Library For Detailed Modeling Of Rocky Exoplanet Internal Structure And Mineralogy

by

Alejandro M. Lorenzo Jr.

A Thesis Presented in Partial Fulfillment
of the Requirement for the Degree
Master of Science

Approved August 2018 by the
Graduate Supervisory Committee:

Steven Desch, Chair
Dan S.-H. Shim
Michael Line
Mingming Li

ARIZONA STATE UNIVERSITY

December 2018

ABSTRACT

The pace of exoplanet discoveries has rapidly accelerated in the past few decades and the number of planets with measured mass and radius is expected to pick up in the coming years. Many more planets with a size similar to earth are expected to be found. Currently, software for characterizing rocky planet interiors is lacking. There is no doubt that a planets interior plays a key role in determining surface conditions including atmosphere composition and land area. Comparing data with diagrams of mass vs. radius for terrestrial planets provides only a first-order estimate of the internal structure and composition of planets [e.g. Seager et al 2007]. This thesis will present a new Python library, ExoPlex, which has routines to create a forward model of rocky exoplanets between 0.1 and 5 Earth masses. The ExoPlex code offers users the ability to model planets of arbitrary composition of Fe-Si-Mg-Al-Ca-O in addition to a water layer. This is achieved by modeling rocky planets after the earth and other known terrestrial planets. The three distinct layers which make up the Earth's internal structure are: core, mantle, and water. Terrestrial planet cores will be dominated by iron however, like earth, there may be some quantity of light element inclusion which can serve to enhance expected core volumes. In ExoPlex, these light element inclusions are S-Si-O and are included as iron-alloys. Mantles will have a more diverse mineralogy than planet cores. Unlike most other rocky planet models, ExoPlex remains unbiased in its treatment of the mantle in terms of composition. Si-Mg-Al-Ca oxide components are combined by predicting the mantle mineralogy using a Gibbs free energy minimization software package called Perple_X [Connolly 2009]. By allowing an arbitrary composition, ExoPlex can uniquely model planets using their host stars composition as an indicator of planet composition. This is a proven technique [Dorn et al 2015] which has not yet been widely utilized, possibly due to the lack of availability of easy to use software. I present a model sensitivity

analysis to indicate the most important parameters to constrain in future observing missions. ExoPlex is currently available on PyPI so it may be installed using pip or conda on Mac OS or Linux based operating systems. It requires a specific scripting environment which is explained in the documentation currently stored on the ExoPlex GitHub page.

To my parents, Alejandro Lorenzo Sr. and Marilu Lorenzo. Without your love and support, I would not have completed this document.

ACKNOWLEDGMENTS

I would like to express my sincere gratitude to my advisor, professor Steven Desch for his professional guidance and friendship over our 6 year relationship. No matter how busy he was, his office door was always open to me and any other student seeking help on academic or life problems or even just to chat.

Thank you to the School of Earth and Space Exploration at Arizona State University and its faculty members for providing a unique environment for the study of planetary sciences. I was part of this program for over 6 years and would not trade my experiences for anything else. I received an exceptional education with no shortage of opportunities for advancement.

TABLE OF CONTENTS

CHAPTER Page

LIST OF TABLES

LIST OF FIGURES

Figure Page

Chapter 1

INTRODUCTION

It has long been speculated that planets outside of our solar system exist. Democritus (460 370 BC) imagined a universe filled with an infinite number of unique worlds. This idea did not fit well with Earth-centric cosmology: Giordano Bruno (1548 - 1600) realized the Copernican theory allows for many more solar systems than was previously thought possible, and thought each star may in fact have planets around them. It would take hundreds of years and countless science fiction stories before exoplanets became a reality.

In the past decade, spaceborne missions such as CoRoT and Kepler [1] have made clear that our Galaxy is filled with more planets than there are stars (Cassan et al., 2012). Accompanying the large quantity of planets now with measured mass and radius is the apparent diversity of exoplanets, many of which have no Solar System analog.

It is of both scientific and philosophical interest to assess the habitability of these new worlds, but this is a challenging task. Given only one model of a habitable planet, we are faced with an inescapable limitation of theoretical ability when discussing the habitability of worlds unlike Earth. As far as we know, life only exists on one planet within a limited range of conditions. With this in mind, it is imperative to develop theoretical models with the current understanding of habitability as a foundation, rather than a limitation, keeping in mind that there may indeed be habitable planets which look very different from Earth.

[1] This research has made use of the NASA Exoplanet Archive, which is operated by the California Institute of Technology, under contract with the National Aeronautics and Space Administration under the Exoplanet Exploration Program.

Habitability is a complex question that needs to take into account everything that can influence the conditions on the surface of a planet; these will include the underlying rocky body (core, mantle, hydrosphere), the atmosphere, and the chemical and thermal exchange between the two. Each layer presents a formidable challenge to model and to relate to data. We focus our attention in this thesis to the solid planet. Most of the available data for rocky planets regard only the solid portion as low-mass planets are not expected to have atmospheres that influence observable properties (Rogers & Seager, 2010; Chen&Kipping, 2017).

Mass and radius, which can be measured to better than 10% accuracy, are the only data points which can be directly tied to the planet. We can relate these to bulk composition through simple models to predict what the interior of a detected planet may be like. Unfortunately this analysis proves to be unreliable beyond only a first-order estimate of internal structure (core and mantle mass fraction). The simplest forward model of Earth, for example, can include as few as four elements—Fe, Mg, Si, and O—accounting for $\sim 94\%$ of Earth by mass (McDonough, 2003). Even with this very simplified composition, it is not possible to constrain the abundance of these elements using only mass and radius. There are more unknown variables than there are data. The situation becomes even more bleak when other refractory elements and a hydrosphere are included. Even so, observations are improving in accuracy, and theory implicating the host star's composition in connection with its planets has proven to reduce the range of possible solutions for forward models of rocky planets (Valencia et al., 2006; Dorn et al., 2015). Catalogs are already in place that make stellar elemental abundances easily available. The Hypatia catalog (Hinkel et al., 2014) currently has abundance data for 365 planet-hosting stars. Open source software that can utilize the available data is, however, lacking.

This thesis presents an open source tool, ExoPlex, that generates forward mod-

els of rocky exoplanets based on their bulk compositions. ExoPlex can be used to assess the mass-radius relationship of planets with arbitrary compositions, thus creating a simple link between the observable host star abundances and the planetary composition.

We continue by briefly outlining the current state of exoplanet studies. As a field deeply motivated by observation, we first discuss the observational methods that are used to find, and infer properties of, exoplanets. The signs of exoplanets are almost always dominated by their host stars; however, clever techniques have been developed to allow for indirect measurement of various planetary properties. Inherent limitations accompany these techniques, which will also be discussed. Following this we will introduce some of the modeling attempts that have been used to answer certain questions in exoplanetology. Purely theoretical forward models which inspired the present work, as well as empirically motivated characterization methods, will be discussed. Our methods are described in chapter 2. In chapter 3 we bechmark our model and discuss various cases. Chapter 4 is a discussion on the assumptions we used and model limitations. We draw conclusions in chapter 5.

1.1 Detection Methods

Astronomical observations rely solely on the light that comes from bodies. The central star in a planetary system is overwhelmingly luminous compared to any planets which may be in orbit. Planets do radiate thermally and reflect stellar irradiation; both types of light can be exploited to characterize atmospheres or detect planets in certain orbital architectures and orientations. But in most cases, the only option is to collect light from the central star and try to infer the presence of planets. A virtually illuminous mass orbiting a central star induces only slight variations in the light received from the star. In most of the methods discussed below, it is these minute

variations which give evidence for the presence of a planet.

It is important to note that for a planet to be confirmed—that is, we are certain that a positive detection is indeed due to an orbiting planet—either more than one of the detection methods must be used, or the evidence using one method must be undeniable after multiple orbits have been observed. The periodic nature of orbits enables the possibility to view systems over through the full range of their movement in the system. If a regular period of variation from nominal conditions appears through several orbital cycles, then it may be clear that some orbiting body is to be the cause. These stellar variations due to orbiting planets are, unfortunately, accompanied by intrinsic stellar variations. Depending on the evolutionary stage and spectral type, variations in luminosity may even preclude the observation of planetary bodies. The regular nature of orbits mitigates some of the inevitable ambiguity in observations. As discussed below, orbital dynamics may even lead to the discovery of more planets for certain types of multi-planet systems. The limitations of current methods of exoplanet detection will be discussed in more detail later in this chapter.

1.1.1 Radial Velocity

As objects orbit one another, they exhibit a mutual gravitational tug that follows Newton's third law. For planets in motion around a star, the induced movement on the central star is hardly apparent; but for detecting exoplanets, this fact of nature is invaluable.

When viewed from an orientation where the line of sight is perpendicular to the orbital plane, planets will appear to approach and recede the observer. Host stars will exhibit similar motion, but to a much smaller degree. By analyzing the spectrum of the host star, this approach and recession is detectable via Doppler shift, and can be converting into a velocity. If an orbiting planet with regular period is indeed

present, the spectrum of a star will show an alternating pattern of blue and red shifts. By observing this motion over a a planet's full orbit, the period P, semi-major axis a, orbital eccentricity e, and the semi-major amplitude of the star's radial velocity, K, can be found. These quantities can be related to the planet mass through the following relationship, from Equation 13 of Lovis & Fischer (2011). Given the mass of the planet, m_p, and the mass of the star, m_s, the semi-major amplitude of the star is

$$K = \sqrt{\frac{Gm_p}{(1-e^2)a}} \sqrt{\frac{m_p}{(m_s+m_p)}} \sin i. \tag{1.1}$$

The semi-major axis a can be found from the observed period using Kepler's third law of orbits:

$$P = \sqrt{\frac{4\pi^2 a^3}{G(m_s+m_p)}}. \tag{1.2}$$

The term $m_p \sin i$ term in Equation 1.1 is due to the orientation of the system where i is the orbital inclination term which is between 0 and $\pi/2$. If viewed edge-on, $i = \pi/2$ and the full consequence of the planet's gravitational tug on the star is seen; otherwise $i < \pi/2$ and we will only be able to partially detect the host star's motion. Without a measure of i, mass determinations from the radial velocity methods are somewhat ambiguous: only a measure on the minimum mass is possible so $m_{\min} = m_p \sin i$. Finding the orbital inclination is an arduous task. It must be inferred from very precise measurements of either photometric transits or astrometry.

Observations of host star spectra tend to be very noisy. Figure 1.2 shows the radial velocity data and accompanying fir for GJ581 c and d (Mayor et al., 2009). The wave form of the star's motion is not always apparent. Statistical routines are necessarily applied in order to find the best-fit periodic function. Figure 1.1, from Figure 1 of Wright and Gaudi (2012), shows the various wave forms that can arise from orbits of different eccentricities and inclinations. In this Figure, the ω term is related to

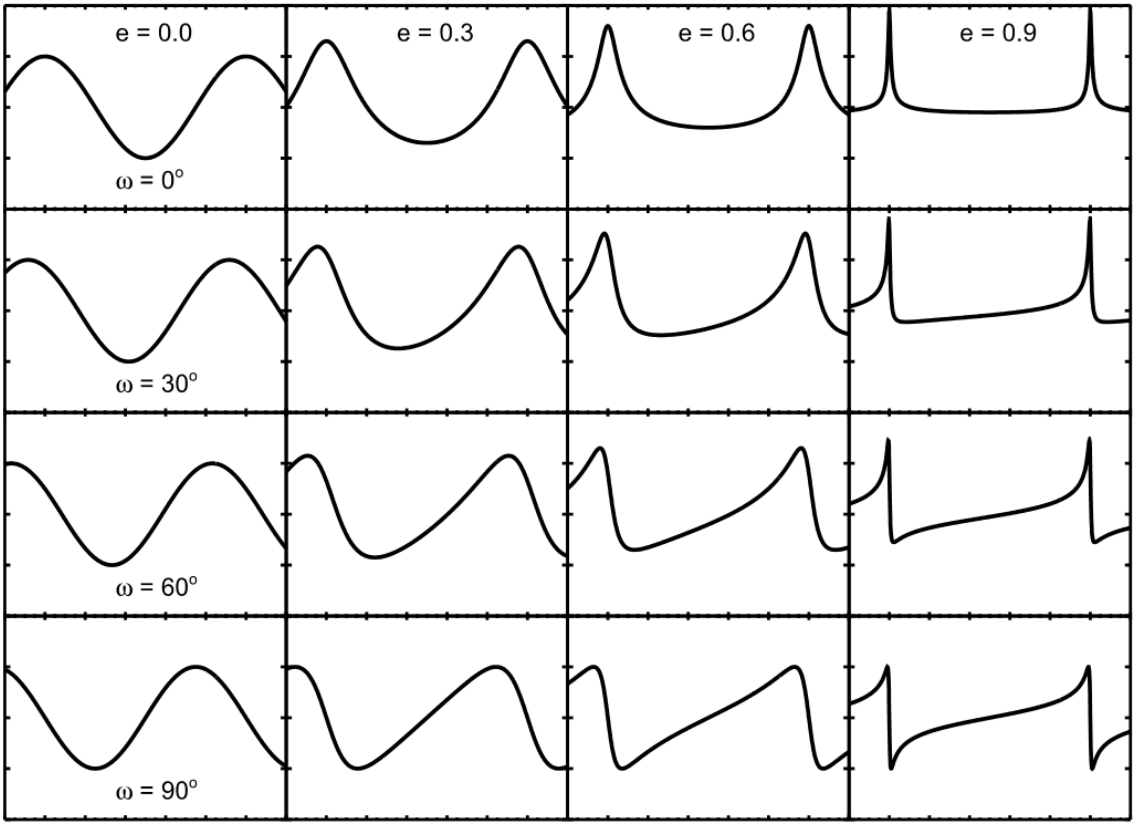

Figure 1.1

Radial velocity periodograms from Wright and Gaudi (2012). They vary the orientation of the orbital plane, ω, and the eccentricity to shop the various wave forms that can be detected.

the inclination. It is interesting to see that from comparing these two figures, we can conclude that the lower planet in Figure 1.2 has a substantial eccentricity whereas the other has a fairly circular orbit.

The magnitude of radial velocity features are of course related to the ratio of the star and planet mass, with more apparent spectral shifts as the mass differential decreases. For the Sun, the radial velocity shift due to Jupiter orbiting at 5.2 AU has amplitude of about 12 m/s, about 30 mphd. Several instruments can reach this sensitivity and better. The HAPRS, ESPRESSO, and SPIRou spectrographs (Mayor

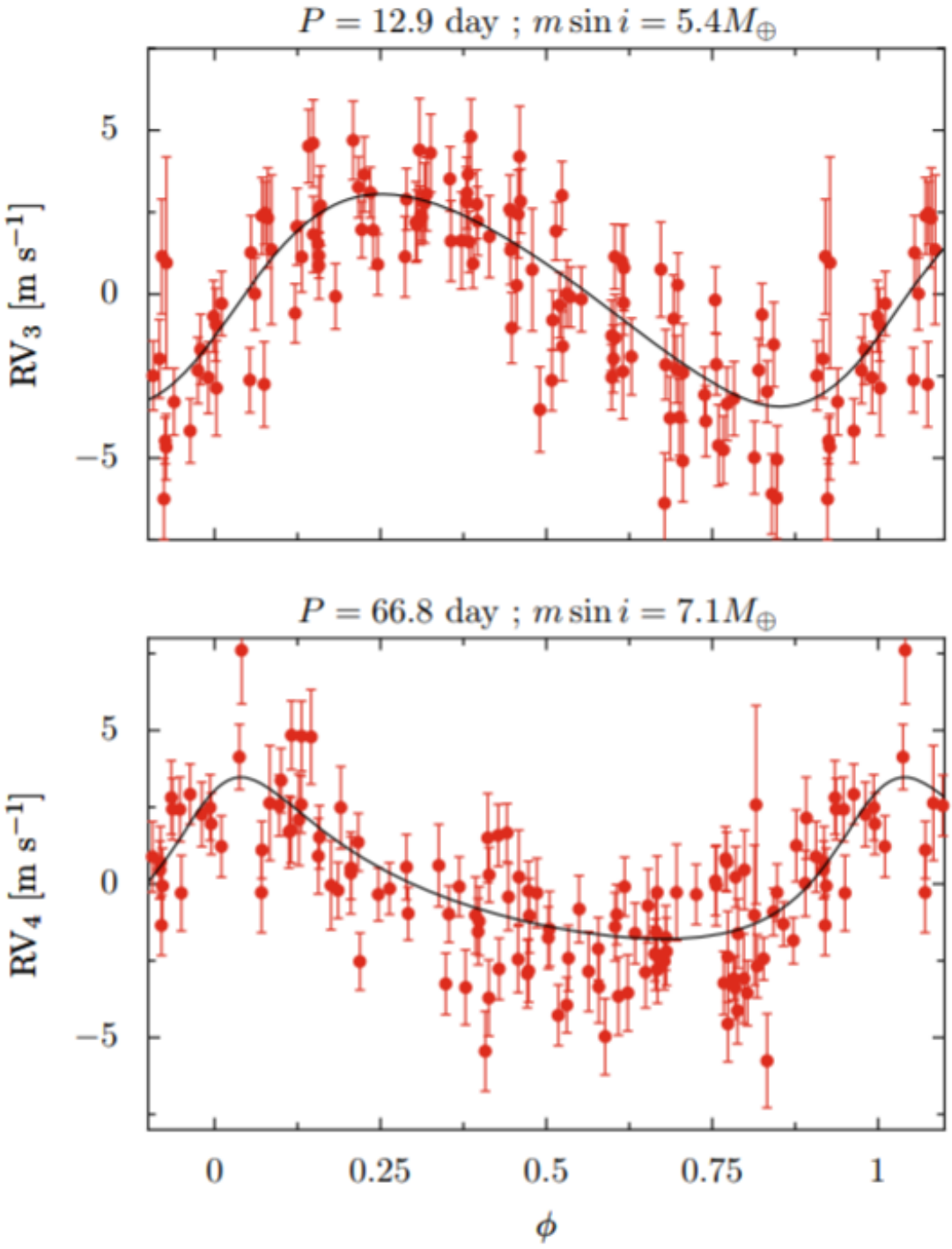

Figure 1.2

Figure from Mayor et al. (2009).Radial velocity data and best fit to the data, for G581c and d.

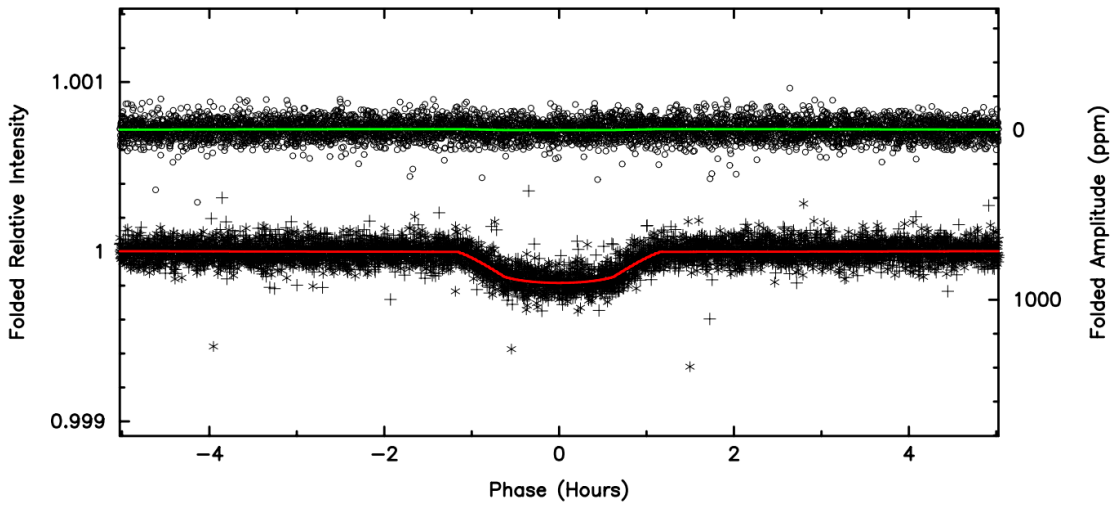

Figure 1.3

Figure Batalha et al. (2011) showing light curve data of Kepler-10. Shown here is the transit (red) and occultation (green) though a full period of orbit for Kepler-10b.

et al., 2003; ESPRESSO SPIE , 2010; Donati et al., 2014) in particular are sensitive to radial velocities of only 1 m/s, just enough to detect planets of about 2 Earth masses near their host stars. Mayor et al. (2009) for example, used the HARPS spectrograph to discover a 1.9 $M_\oplus$ planet with a 0.03 AU semi-major axis in orbit around the M dwarf GJ581.

1.1.2 Transit

The most robust method of finding the radius of an exoplanet comes from the blockage of a fraction of the light received from a host star as a planet passes in front of the star along the line of sight. Being essentially illuminous, the planet blocks an area that is proportional to its radius squared, so the amount of light blocked follows the relationship

$$\frac{\Delta F}{F_\star} \simeq (R_p/R_\star)^2$$

For larger planet radii R_p, the reduction in flux, ΔF, is greater. So the transit method is biased towards systems with a larger planet to star size ratio.

The transit method is easily understood assuming a uniformly emitting light source. Unfortunately, this isn't the case. In practice, stars are dynamical light sources that have intrinsic variations that can be greater than the dip in brightness from a planet. Earth, for example, would account for just a .00839% dip in brightness, whereas sunspots can appear with a diameter several times that of Earth and lead to greater dips. Given enough time to view multiple periods of an orbit, however, transits may be delineated from stellar blemishes. This requirement forces a bias towards shorter period planets. Signals are often so weak that probabilistic routines are used to find the best-fit transit curves. Figure 1.3 from Batalha et al. (2011) shows data of the light curve of Kepler-10b through a full phase. A total of 19 periods were observed over four months in this monumental first discovery of a rocky exoplanet.

Not all systems are accommodating to the transit method. A certain orbital alignment is required for the transit method to be applicable. An edge-on orbit, with an inclination near 90 degrees, is required. It is highly improbable for this to be the case. Stars are randomly distributed in rotation axis even within star-forming regions, and the planets which form around stars tend to all orbit along the same orbital plane and direction as the star's rotation. For the highest probability of detecting a transit, the maximum separation of the star and planet (semi-major axis) must be less than the sum of the planet and star radii (Wright and Gaudi , 2012), introducing a bias towards planets with more compact orbits.

Because mass and radius are both required to characterize an exoplanet, an exoplanet must be observed by both the radial velocity and transit technique. These two methods provide mass and radius, respectively, and are somewhat complementary techniques, although both have biases toward large planets and short periods

/ close-in orbits. About 1/3 of transiting planets have measured minimum or true mass, found by measuring their Doppler shift after discovery through transits.

With observations of only the accumulative light from a host star, much needs to be inferred before one can make even an estimate of the planet radius from periodic light depletion. The most ideal conditions permit transit photometry from the ground at a reasonable cost, but inevitably yield some error in the estimation of the ratio of planetary radius o stellar radius. Of course, without knowledge of the stars radius, deriving a planet's radius from transits would be impossible. A direct measurement of most stars' radii is not currently possible, but can be estimated from theory. The stars spectral type can be found and then compared with synthetic spectra to constrain the stellar mass and radius. With all uncertainties accounted for, the current data yield an average radius error for confirmed planets with radii less than 1.5 $R_{\oplus}$ of about 20% (n=672), an impressive mark of accuracy given the details discussed in this section, but still leading to many degeneracies in planet properties. This work and many others serve as a step beyond these observational limitations by modeling artificial planets and comparing them to additional available data.

One type of additional data may be composition. Some transiting planets may also be good targets for transit spectroscopy where their atmospheres may be characterized. The difference in the spectra between the primary transit where the planet passes in front of the star and when the planet is behind the star, reveals what stellar light has passed through and had been attenuated by the planet's atmosphere, giving clues to its composition and temperature structure. One of the first transiting planets discovered is HD 209458b, a hot-Jupiter orbiting a sun-like star (Charbonneau et al., 1999) was also the first planet to have its atmosphere analyzed through transit spectroscopy.

1.1.3 Timing Methods

Massive objects interact with each other through mutual gravitational attraction. As previously discussed with the Doppler method, these gravitational perturbations can give way to enough clues in observed light to infer the existence of exoplanets; combined with the regular, periodic nature of orbits, timing methods are a robust source of detection. There are two methods in use: pulsar timing (if the planet orbits a pulsar) and transit timing variations (if there are multiple planets in the system). Because these features are due directly to massive objects, these timing methods allow observers to infer the mass of planets with considerable accuracy.

If the beam of a pulsar is along the line of sight (a rare occurrence in itself) then the pulsation period may be measured. Pulsars survive for on the order of tens of millions of years before they slow down enough to extinguish and are no longer luminous. Thus on human timescales, these objects are stable and regularly pulsating. Any variation of the pulse then can be taken as anomalous. Objects in orbit about a pulsar can periodically, alter the regular intervals of the pulsar, thereby allowing obervers to infer the object's mass. While relatively rarely used, the first exoplanets to have been confirmed, PSR B1257+12b and PSR B1257+12c, were found around a pulsar (Wolszczan et al., 1992). To this day these are still some of the smallest planets ever discovered. Following these discoveries, PSR B1257+12a, the least massive exoplanet known, was found in the same system (Wolszczan A., 1994).

Like the pulsar timing method, inconsistently transiting planets give clues to additional planetary companions. Systems of multiple planets can fall into phase equillibria due to the mutual gravitational pull of the planets in addition to the pull of the central star. Even if planets are not found through transits due to their small size or long periods, they may be inferred from irregular orbits of one or more tran-

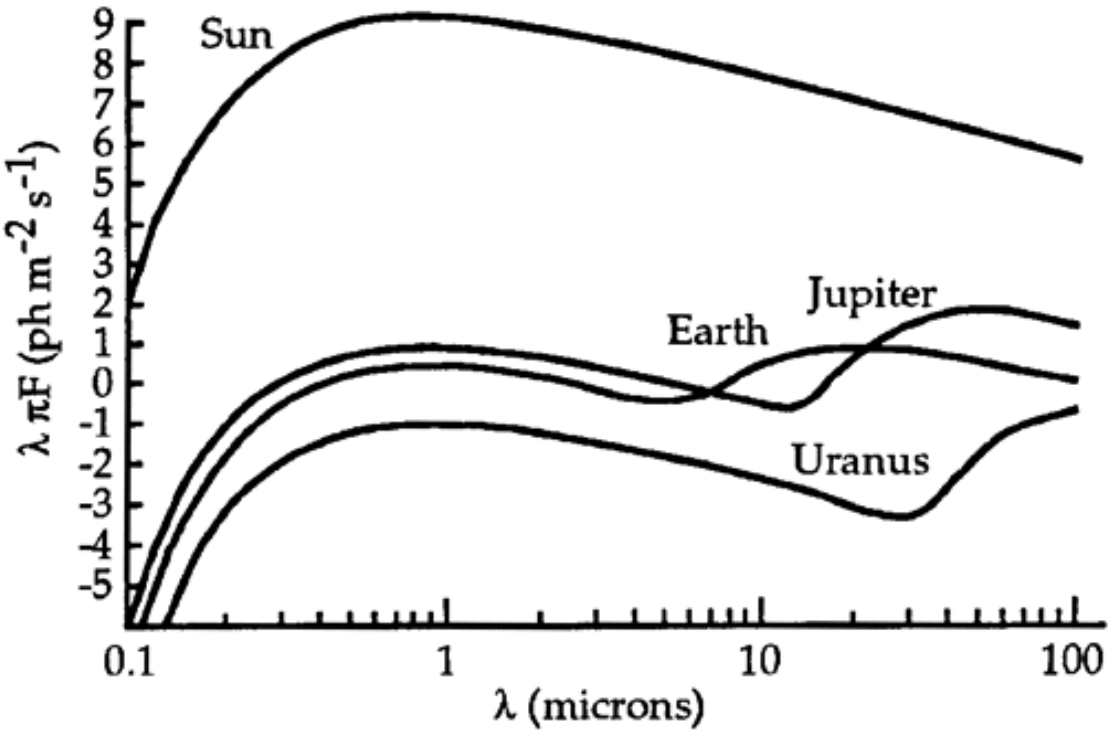

Figure 1.4

Relative fluxes of the Sun, Earth, Jupiter, and Uranus, as a function of wavelength. Image credit: Michael Richmond (RIT)

siting planets. Such was the case for the TRAPPIST-1 system (Gillon et al., 2016, 2017) where the planets of the system had measured radii from transit and measured masses from transit timing variations. The orbital resonances in combination with other inferred orbital characteristics allowed for highly accurate mass measurements.

1.1.4 Direct imaging

The only method where the planet is actually in view is the direct imaging method. Planets themselves emit very little light. Some of this radiation comes from thermal emission while the rest is reflected stellar light. Contrasting the light between the planet and host star is, in most cases, impossible. The star is overwhelmingly lumi-

nous. The Sun, for instance, is 8.5 orders of magnitude more luminous than Earth in visible wavelengths, as illustrated in Figure 1.4. However, there are techniques and certain cases which permit direct imaging. The ideal conditions for this method do not converge with the requirements for detection with other methods; directly imaged planets are found and studied with solely this technique.

For a successful observation, planets must be far enough from their host star to resolve. The limiting distance depends on how much light the planet reflects and the host star luminosity. In general, a semi-major axis of more than a few AU is necessary. Instrumentation designsed for the task uses a coronagraph to block the stellar light to enhance contrast between the two bodies. Normally, this method is practical only for very large, gas-giant planets. To extract the most information from a system, the orbital plane should be face-on so the entire orbit is visible. In this case, an estimate of the planets mass is possible, along with other orbital parameters. Very rough estimates of the planets radius are possible, albeit with a significant ambiguity. The most beneficial observation made possible by directly detected planets is a spectral analysis of the planets' atmospheres. These observations offer the most conclusive evidence available on the composition of exoplanets. This has motivated the development of new direct detection campaigns on the ground. Space-based observatories equipped with coronagraphs have been proposed as well.

1.1.5 Summary of detection methods

Table 1.1 lists the aforementioned exoplanet detection methods along with the parameters they aim to measure, and the number of confirmed detections to date (July 2018). The most successful procedure for finding and extracting information on exoplanets has been to make first detection with spaceborne missions like *Kepler* or the recently launched *Transiting Exoplanet Survey Satellite* (TESS), which observe

tens of thousands of stars at once, looking for dips in photometric signals that may hint at a transiting planet. At that point, radius and orbital parameters are known. Often, follow-up observations with the radial velocity technique can be made to find mass of transiting planets.

Biases in these methods should not be overlooked. Both the transit and radial velocity methods strongly favor a quiescent star whose planets have a small orbit. M-dwarfs are not favorable for the radial velocity technique because they have very active photospheres (Tian & Ida, 2015) that can wash away spectral signals; however, M-dwarfs may be ideal for transit detections due to their small size, which means proportionally stronger transits. Atmosphere spectroscopy can be performed for some transiting planets and also for directly detected planets, but not for both. Direct detections require a face-on orbital orientation of a system with a large planet that's distant enough from its host star to resolve.

Table 1.1

Detections methods and how many times they appear in published works of confirmed exoplanets. Data compiled by the NASA Exoplanet Archive.

Method	Parameters gained	Detections
Radial velocity	minimum mass, orbital period, eccentricity	673
Transit	radius, orbital period, estimate of inclination	2919
Direct imaging	orbital parameters, atmosphere spectra	44
Timing	mass, semi-major axis	32*

*Transit, pulsar, and eclipse timing variations

1.2 Exoplanet models

Measurements on mass and radius have clearly come a long way. Thousands of planets are now known to exist and it seems that exoplanets are ubiquitous. Moving beyond detection, the focus is now on the characteristics of exoplanets themselves. Most exoplanets will, at best, have a mass and radius measurement each with about a 10% uncertainty (most often higher). This provides a measure of the bulk density of the planet (because $\rho \propto M/R^3$) which can be compared to the solar system planets, of which we know much more about than the typical exoplanet. If the bulk densities are similar to any of the solar system planets, it can be inferred that the observed exoplanet shares similar characteristics. Earth, Neptune, and Jupiter are each unique planet types. With bulk densities of 5.51, 1.64, and 1.33 $\mathrm{g\,cm^{-3}}$ respectively, it is relatively easy to group observed exoplanets into these populations to determine if a planet is rocky, icy, or gaseous. A caveat to this type of analysis is that it assumes observed systems mirror our own planetary system, a paradigm that was shattered with the first exoplanet discoveries.

Observation alone is insufficient to characterize exoplanets. We thus turn to models that can be compared to observation in order to find qualities consistent with planetary types. Essentially we want to know what planets are made of. Unfortunately, these models are highly degenerate. In the simplest case, a model of Earth can be made my mixing the proportion of core, mantle, and hydrosphere. While one might find that a model with 33% core, 67% mantle, and 0.02% water will produce Earth exactly, so too will other combinations of those three layers. With only two data points (mass and radius), we cannot possibly constrain the values of three parameters. Furthermore, each layer will have a different reaction to self-compression. Some materials are much more compressible than other, which further complicates

solutions. Degeneracies can be relieved somewhat by making reasonable arguments. For example, Earth-mass planets made entirely of mantle and water or made purely of core materials, probably do not exist.

Our best hope of constraining the composition of planets is to make forward models that take in all of the measurable details of planetary systems. Here we will review the work that has been done which lead to our current understanding of rocky exoplanet compositions.

1.2.1 General modeling approach

Models begin with certain assumptions that stem from the available data on the solar system planets. The limited and incomplete data available no doubt influence theory of the nature of exoplanets. We can only work from what we already know and extrapolate from there, albeit with caution. Arguments from planet formation theory seem to support the universality of the mechanisms which have led to the internal structure of the terrestrial planets. As such, it is believed that rocky planets are structured such that they have an iron-dominated core, silicate mantle, a water layer, and an overlying gaseous envelope. The latter two are less significant for low-mass planets less than a few Earth masses (Rogers & Seager, 2010; Chen&Kipping, 2017).

Silicates and metallic iron condense within 50 K of each other in the solar nebula (Lodders, 2003). They should both exist within planets forming near their host protostar. The latter two layers however, are delivered to close-in planets by other mechanisms that are more difficult to constrain. Their presence on an exoplanet is not even guaranteed. Planets of nominal mass have little ability to keep a gravitationally bound atmosphere: depending on stellar insolation, set by the distance from the host star and the stars luminosity, the ability of a planet to hold onto an atmosphere against thermally driven escape may be very low. Solar insolation may also prevent

surface water by evaporation, photodissociation and subsequent thermal escape.

Formation environment determines the eventual composition of the planet. If the planet forms beyond the radial distance from the central protostar at which water condenses as ice, the planet may accrete a substantial fraction of its final mass in water. Otherwise, the planet might not form with enough water to impart a detectable influence in the planets bulk density.

Earth serves as the only complete example available for comparison to other rocky planets. As such, models make the assumption that exoplanet mantles will have compositions similar to the Earth's, i.e., mostly silicates. This assumption is further supported by the similar condensation temperature of Fe, Si, and Mg in the solar nebula. These elements, along with O, account for about 94% of Earths mantle (McDonough, 2003). How these elements are distributed in the mantle and core in models is discussed below. Before that discussion, it is prudent to understand the general approach taken in every theoretical model.

Exoplanet models mirror the approach taken by Zapolsky & Salpeter (1969) who modeled homogeneous spheres and found a power law relationship relationship between mass and radius,

$$R \propto M^a$$

, below a critical mass (hundreds of Earth masses) at which $a = 0$. At higher masses, all materials are significantly compressible and additional mass will lead to smaller radii. Rocky planets, at much smaller masses, follow a power law with $a > 0$.

The Zapolsky & Salpeter (1969) model, and current exoplanet models, all rely on at least four fundamental equations, along with the assumption that planets are spherically symmetric and thus only vary along the radial direction. The one-dimensional

equations are:

$$\frac{dM(r)}{dr} = 4\pi r^2 \rho(r) \tag{1.3}$$

$$g(r) = \frac{GM(r)}{r^2} \tag{1.4}$$

$$\frac{dP(r)}{dr} = -\rho(r) g(r) \tag{1.5}$$

$$P(r) = f(\rho(r), T(r)). \tag{1.6}$$

These equations set the conditions for equilibrium. They are mutually dependent and solved as a function of radius (r) within the planet. Hydrostatic equilibrium is the backbone of a planet model which determines steady solutions. Gravity is solved with the familiar Newton equation. Finally, an equation of state is necessary to relate density with pressure and temperature at various depths within a planet. Boundary conditions regarding the pressure differ from model to model; however, by splitting the planet into successive shells and setting the central mass to zero, these four equations can be coupled and solved iteratively until these equations are in equilibrium.

Equations of state (EOSs) are necessary to calculate the self-compression that occurs within planets due to overlying material. The two most commonly used relationships are the Vinet (Vinet et al. , 1987) EOS and the Birch-Murnaghan equation of state (BME) (Birch , 1947). The Vinet EOS is

$$P = K_0 \, \eta^{2/3} \Big(1 - \eta^{-1/3}\Big) \, \exp\left[\frac{3}{2}\Big(K_0' - 1\Big)\Big(\eta^{2/3} - 1\Big)\right]. \tag{1.7}$$

The BME is obtained by a series expansion of an expression for the free energy. It is used as an expansion to the second, third and fourth order. The third-order BME, or BME3, is

$$P = K_0 \Big(1 - \eta^{7/3} - \eta^{5/3}\Big)\left[1 + \frac{3}{4}\Big(K_0' - 4\Big)\Big(\eta^{2/3} - 1\Big)\right]. \tag{1.8}$$

The fourth-order expression for the BME, or BME4, is

$$+\frac{3}{2}K_0\Big(1-\eta^{7/3}-\eta^{5/3}\Big)\frac{3}{8}K_0\left(\eta^{2/3}-1\right)^2\times\left[K_0K_0''+K_0'\Big(K_0'-7\Big)+\frac{143}{9}\right]. \quad (1.9)$$

In Equations 1.7-1.9, $\eta=\rho/\rho_0$ is the ratio of compressed density to the same material in ambient conditions, ρ_0. The (isothermal) bulk modulus,

$$K_0=-V\left(\frac{\partial P}{\partial V}\right)_T$$

and its first pressure derivative, $K_0'=\partial K_0/\partial P$, appear in both the Vinet and BME with the second pressure derivative of bulk modulus as a component of the BME4. In practice, bulk modulus is not measured directly, but the EOS more directly is and the bulk modulus derived from it. Thus, a reported bulk modulus that assumed the Birch-Murnaghan EOS should not be input into the Vinet EOS, and vice versa, or else significant discrepancies may be introduced.

Various models depart from one another in the choice of composition for the core and mantle layers and their corresponding equations of state. For example, Earths core is predominantly liquid iron, yet many models will choose a solid state of iron for their cores. The core in most models is fixed at one phase because materials at core pressures and temperatures are not well understood. For the mantle, some models account for phase changes, but most do not. Earths mantle exhibits crystallographic reconfigurations of lower-pressure minerals as pressure increases with depth. These features are conspicuous in seismic data yet are often neglected in models of the bulk planet. The upper mantle of Earth is dominated by olivine. Below 410 km depth, the olivine transforms to wadsleyite. Deeper into the mantle, ringwoodite appears. Below 660 km depth, the original chemical composition breaks down into bridgmanite and periclase. Further down into the mantle bridgmanite transforms into the denser post-perovskite phase. These phase changes within Earth and their corresponding pressure

boundaries are summarized below (Helffrich & Wood, 2001; Ito & Takahashi, 1989; Liu, 1976):

$(Mg,Fe)_2SiO_4$	$\rightarrow$	$(Mg,Fe)_2SiO_4$	13-14 GPa	Not all
Olivine		Wadsleyite		
$(Mg,Fe)_2SiO_4$	$\rightarrow$	$(Mg,Fe)_2SiO_4$	18 GPa	
Wadsleyite		Ringwoodite		
$(Mg,Fe)_2SiO_4$	$\rightarrow$	$(Mg,Fe)SiO_3$ + $(Mg,Fe)O$	23 GPa	
Ringwoodite		Perovskite Magnesiowüstite		

models consider these transformations. Indeed, Earths mantle is predominantly perovskite and its bulk density can be well predicted in this simplified view.

Below, I will discuss two regimes of exoplanet models that have been published since 2004. The research goals differ between studies and the models they create reflect this. First, I will discuss the simplified models which do not consider mantles with pressure- and temperature-dependent phase changes. Following this, I will move on to the more sophisticated models. Each regime has its place in exoplanetology, motivated by the vast parameter space of possible compositions and internal structures.

1.2.2 First-order models

The expected diversity of exoplanets can lead to a chaotic modeling space. With only noisy data of mass and radius, it is difficult to perform rigorous compositional analysis on confirmed planets, even in the best cases. Simpler models have illuminated this issue. I define a first-order model as one which does not seek to explore the parameter space of possible mantle composition. These models tend to avoid the nuances of mineralogical phase changes in favor of a homogeneous mantle description with limited mineral diversity; often with one or two mineral phases used to describe

the density at a given depth. Despite the lack of detailed mineralogy, a simple model can provide an accurate description of the bulk density of a planet, essentially fitting the available data on a planet (mass and radius) and offering a suitable solution for the internal structure. While a solution for the core and mantle mass fractions is attainable, it is often hardly the only possible configuration. Degeneracy arises once a more detailed description of composition is sought.

The solution degeneracy for the two data point scenario was exposed by several groups. Seager et al. (2007) developed a useful mass-radius diagram (shown below in Figure 1.5) which allowed comparison of bulk densities with synthetic curves over a range of simple models from purely solid Fe to purely hydrogen. Between these extremes, the rocky and sub-Neptune planets fit.

Their goal was to make a simplified model of exoplanets which uses only temperature-independent equations of state. These so-called cold planets are fixed at 300 K throughout. Equation-of-state data are often more available and better studied at room temperature. So, for pressures within the ranges explored experimentally, these formulations are within empirical results from compression experiments. Additionally, temperature effects are nominal for a homogeneous mineral phase. Pressure is the dominating parameter with respect to a planet's internal density gradient. For each layer (core, mantle, etc.), Seager et al. (2007) selected a single material. For the most part, they chose the higher-pressure polymorph of the material and just compressed it using either the Birch-Murnaghan (BME) or Vinet EOS. The mantle was described entirely by silicate perovskite (bridgmanite), $MgSiO_3$. Earth's mantle is largely composed of bridgmanite (Helffrich & Wood, 2001) but not entirely. The upper mantle, above a depth of about 660 km, is composed of minerals with lower density. Using this model on the Earth means that at least 10% of the radius will be predicted to have a lower density and mass. The reference density of bridgmanite

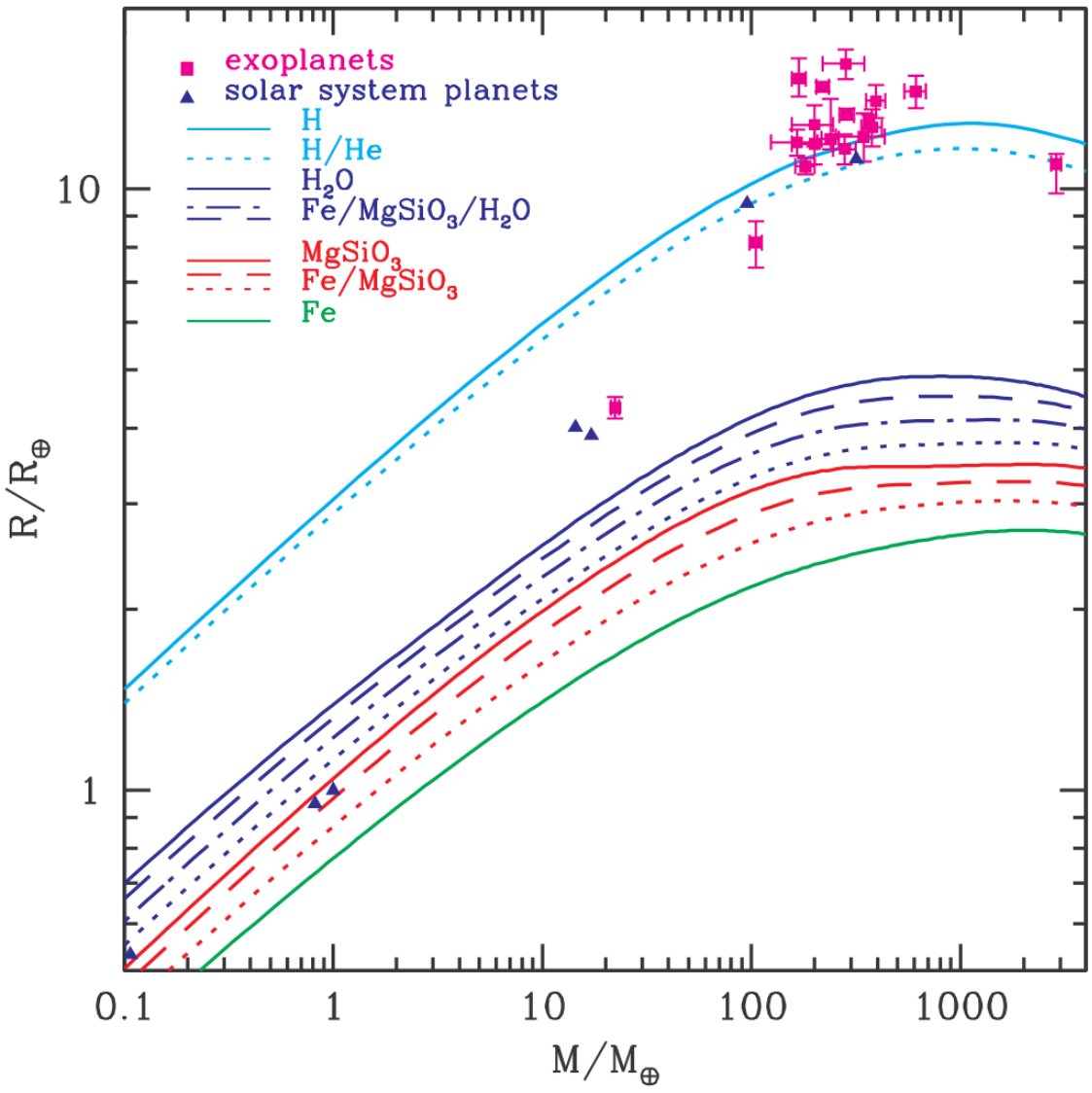

Figure 1.5

Figure 4 from Seager et al. (2007). Mass vs. radius diagram (normalized to Earth mass and radius) for planet compositions from 100% Fe to pure H. These curves represent the mass-radius relationship for planets of uniform composition. Rocky planets like Earth will fit between the 100% $MgSiO_3$ curve (red) and the 100% Fe curve (green).

is about 20% higher than that of olivine so the volume would be in error by this amount. The thickness of the upper mantle would then be over-predicted by about 6% because $R \propto V^{1/3}$. Since this error is only in 10% of ther planet, the overall radius would be in error by only 0.6%, well within observational errors of radius. So using just a high-pressure phase of mantle minerals will yield a reasonably accurate model of mass and radius. While imprecise in their methods, the Seager et al. (2007) model was able to provide a first-order estimate of what new worlds were composed of. This effort has aided in understanding the frequency of various planet classes and has helped to shape current and future observation campaigns.

Seager et al. (2007) also extended their model to cover extreme masses. They connected conventional low-pressure equations of state to the Thomas-Fermi-Dirac theory-based equation of state at extreme pressures. While they extrapolated the terrestrial planet to well beyond the critical self-compression limits where additional mass reduces the radius, this served as a boundary for what would be the case if a rocky planet were to have such an extreme mass, an important exercise in a still very young field of study.

Subsequent studies have considered the composition of planets in more detail. Sotin et al. (2007) sought to find the mass-radius relationship for a variety of super-Earth compositions. They explored the idea that a planet mirrors its host star's composition, at least for the refractory elements Fe, Si, and Mg. The relative elemental ratios of Fe/Si and Mg/Si are included as inputs through stoichiometric arguments because these all exist as primarily oxides in Earth. The proportion of iron and magnesium are easily considered by fitting the molar contribution of each into silicate minerals in the mantle. (Note that iron and magnesium can substitute for each other in silicates, as in $(Mg,Fe)_2SiO_4$, for example). This study was limited to solar composition and they explored the addition of 50wt% of H_2O above a solar composition

rocky interior. While they introduced a new way to constrain the composition of rocky exoplanets with the relation to host star composition, they exposed up a new set of degeneracies which are difficult to overcome.

Another interesting study came from Valencia et al. (2006, 2007b) in which they created a state-of-the-art model for Earth and scaled up their model to 10 $M_{\oplus}$ planets. They defined a super-Earth planet to have a mass between 1-10 $M_{\oplus}$. Valencia et al. (2007a) applied this model to characterize what was possibly the first discovered super-Earth planet, GJ876d (Rivera et al., 2005). To this end, their model increased the rigor to create a highly detailed internal picture of massive rocky planets while maintaining many of the assumptions made by Seager et al. (2007) and others. That is, they fixed the mantle composition, noting the trivial impact of varying proportions of silicates with magnesium- and iron-bearing oxides. They used only Mg, Si, O, and Fe in their mantle. To decide the proportion of each and test the effects of Fe in the mantle, they varied the mantle Fe content and the molar percentage of Fe in magnesiowüstite, $(Mg_{1-\chi},Fe_{\chi})O$ (wu). They found that 10% Fe and 30% wu best fit the Preliminary Reference Earth Model (PREM). Similarly, they made a fit to the PREM to find the best core composition. In Valencia et al. (2007a), they used $Fe_{0.8}$ $FeS_{0.2}$ to model GJ876d. Unlike Seager et al. (2007), they used temperature-dependent equation of state data. For the temperature gradient, they modeled an internally self-consistent geotherm including a radiogenic contribution to the heat budget. They used this to find the thickness of the core-mantle and mantle-surface boundary regions where heat transfer is through conduction rather than through (adiabatic) convection.

Valencia et al. (2006) tested a variety of core compositions, noting the importance of alloys in finding the liquid-solid core fractionation that best represents seismological models of Earth. To this end, they include a solidus model for pure Fe and the alloys

FeO, FeSi, and FeS. Interestingly, they found for planets more massive than Earth, the core remains in a solid state. However, by varying the Grüneisen parameters in the solidus equation they used or by using a hotter but still reasonable geotherm, they were able to have partially liquid cores for the entire range of masses they modeled (1-10 $M_{\oplus}$). This implies that finding core states is a difficult task and also that in most cases liquid cores cannot be ruled out.

With no radius estimate, Valencia et al. (2007a) were able to explore the range of internal structures compatible for GJ876d, with a mass of 7.5 $M_{\oplus}$. They found that if its radius were less than 9,600 km, this planet would not contain a significant volatile layer, whereas if the planets radius were measured to be greater than 12,000 km then it would need to contain at least 20% H_2O by mass. Between these radii, a continuous range of internal structures could fit the mass and radius. To illustrate the dilemma, Figure 1.6 (from figure 4 of Valencia et al. (2007a)) shows the trade-off between core mass fraction and H_2O mass fraction. Along the solid curve, each composition fits the mass of GJ876d and its proposed radius of 11,900 km.

The data available on exoplanets of this mass have immensely improved in quality and volume since this work. We know now that at such a mass, GJ876d is unlikely to share Earth's exact composition. Indeed, Valencia et al. (2007a) argue that it is likely this planet does contain a significant volatile mass fraction, but this was not empirically testable at the time. As exoplanetology has evolved, theory has been developed along-side observation, and while degeneracies still remain, it is clear that progress has been made in constraining the composition of rocky exoplanets.

Rogers & Seager (2010) quantified the solution degeneracy for rocky exoplanets in high- and low-bulk-density regimes. They coupled an atmosphere model with a rocky planet model from Seager et al. (2007). They tested the degeneracy of exoplanet models in constraining the composition of confirmed planets. By using only

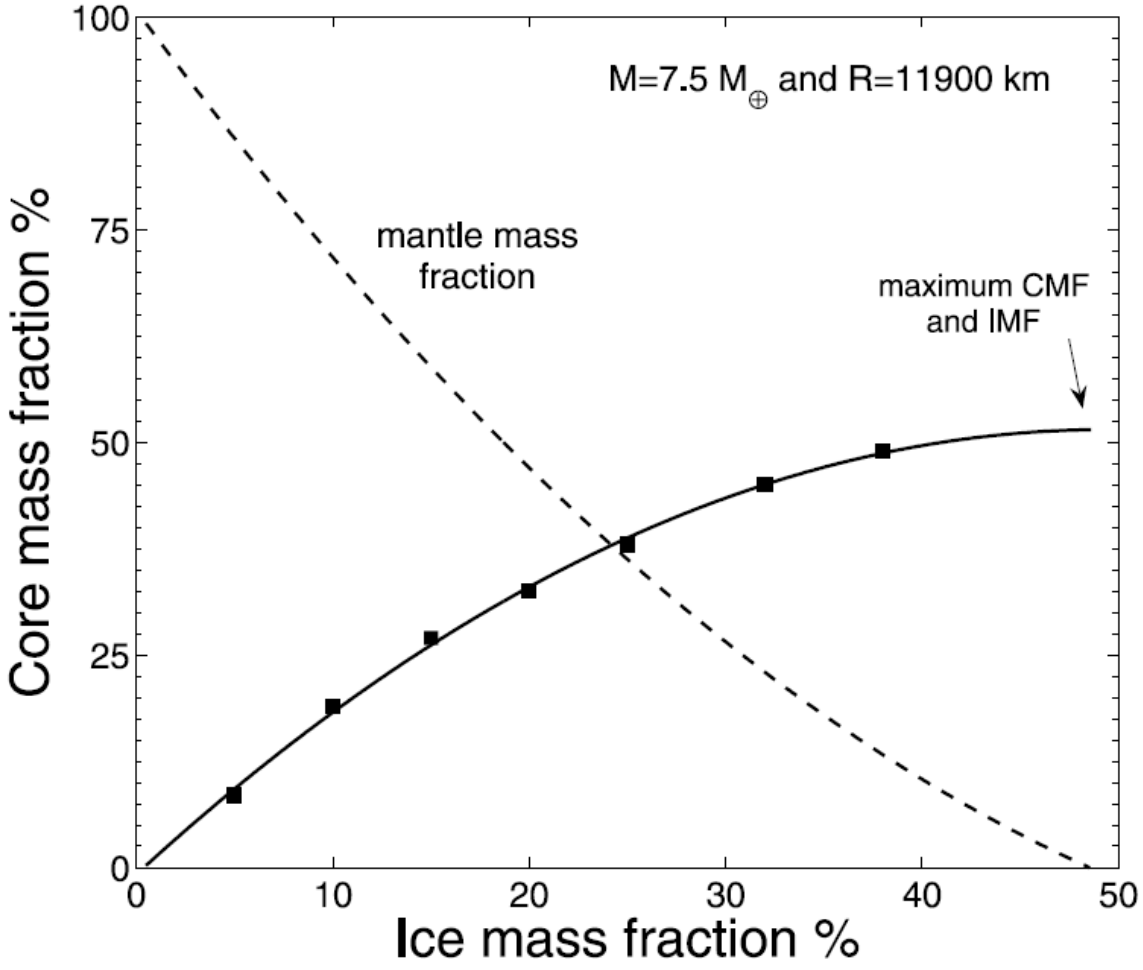

Figure 1.6

Figure 4 from Valencia et al. (2007a) Trade-off diagram for possible internal structure of GJ876d if its radius were $R = 11900$ km. Each point on the solid line is a possible solution that yields the same mass and radius. The solid line connects possible points of core and ice mass fractions and the dashed line is the corresponding mantle mass fraction. Possible core and ice mass fractions range from 0 to 50%.

mass and radius, they found that the level of model degeneracy is sensitive to planet bulk density. Denser planets, within the density regime of terrestrial planets, are best described assuming little to no volatile or water layer. Removing these dimensions constrains the first-order problem to just solving for the planets internal mass distribution between the core and mantle. With a well-constrained mass and radius, it is possible to find a unique solution for the core and mantle mass fractions. To higher order, denser planets are more amenable to assertions involving the more detailed composition of the mantle. While this and all other exoplanet model papers have found the bulk radius of a rocky planet is insensitive to various mantle abundances of Si, Fe, and Mg, Rogers & Seager (2010) quantified this and proved that the best chance of studying exoplanet mantles in detail is to look at the denser planets found.

There is no doubt that the diversity of planets in the Galaxy extends beyond what is seen in our solar system. The first two planets to have been discovered were unlike anything seen before: a planet around a dead star, and a gas giant on a 4-day orbit. Creative minds thrive in such an uncertain and new landscape as exoplanetology. One such exploration into new types of planets came from Léger et al. (2004), who used a simple model to study the possible surface conditions of "ocean planets". It was proposed that ocean planets have an extensive H_2O region which would be detectable, or at least not ruled out, by the planets bulk density. Lower bulk densities, for example, would appear closer to the 100% H_2O curve in Figure 1.5. In some cases, a model with only a core and mantle could be ruled out entirely based on a low observed bulk density. This is in contrast to the case of denser planets, where it would be impossible to determine that Earth has a water mass fraction of about 0.02%.

Léger et al. (2004) explored ocean planets with masses $< 8M_{\oplus}$. Below this mass, it is expected that these planets can not hold on to an atmosphere extensive enough to

impact observation of planetary radii. They asserted that many ocean planets would form just outside of the snow line and within the radius where methane and carbon monoxide condense. They considered what would happen if such a planet migrated into the habitable zone where the amount of stellar insolation received is sufficient for the existence of liquid surface water. In their model, ocean planet volatile content are similar in composition to comets: mostly H_2O (90wt%) with some NH_3 (5wt%) and CO_2 (5wt%) where the H_20 is present entirely in its own layer and the rest is represented in a gaseous envelope. The ice layer is simply ice VII because it appears for a much larger range of temperature and pressure in the water phase diagram than other ice phases. When necessary, they extrapolated the Fei et al. (1993) equation of state for ice VII beyond 20 GPa. For the underlying rocky planet, the core is a Fe-Ni alloy in a solid state and the mantle is similar to Seager et al. (2007) but with a different equation of state. To evaluate the state of the H_2O, liquid or ice phase, they included an internal adiabatic temperature gradient along with a two-stream model of an atmosphere consisting of N_2 and CO_2. They varied stellar insolation and the mass fraction of the core and water layers to find the possible radial extent of surface oceans. In doing so, they found that it is possible to have planets with liquid water surfaces that extend up to about 100 km in depth.

First-order models have served as a valuable component in analyzing observed exoplanets. They all follow similar assumptions that rocky planets are composed of two layers: Fe-dominated core and a silicate mantle composed mostly of $MgSiO_3$. Extending these models to include volatiles allowed for comparison to some of the larger planets discovered. It turns out that exoplanets larger than a few Earth radii must contain a significant volatile layer. On the other hand, smaller, denser planets are less likely to have an extended atmosphere and water layer. This breaks the problem down into the mass contribution between two layers. Because detailed composition

has little influence on overall radius, simplified core and mantle composition can be used to find a first-order constraint on the internal structure of dense planets. Moving forward, understanding more about the composition of core and mantle layers requires a more sophisticated approach. In the next section, we will discuss such models.

1.2.3 Higher-order models

The models introduced in the last section were devised in a time where the pace of exoplanet detections was rapidly increasing. Following an explosion of confirmed planets, it became more viable to not only study the bulk statistics of nearby planets but also to investigate individual exoplanets in more detail. It is clear now that despite observational biases there is no lack of diversity of exoplanets among current catalogs. This includes planets of density like Earths which may closely resemble the Earth and serve as targets for further habitability analysis. On the other side of the coin, Earth-mass and -radius planets may not resemble Earth at all. A more detailed picture of what planets look like inside and in turn how they behave geophysically and geochemically will be necessary to come to any conclusions describing surface conditions. The following models show a marked shift in focus to more sophisticated descriptions of planet interiors, including multi-mineralic models of the upper and lower mantles of rocky planets. The ability to model planets of arbitrary composition is another vital feature of a modern exoplanet model. The composition of host stars can play a role in constraining the composition of its planets.

We consider the model of Valencia et al. (2006), discussed above, to be a first-order approach because they did not allow for varied composition of their mantle and core. They did, however, include mineral phase transformations as a function of pressure and temperature. As discussed below, modeling phase changes is a formidable task.

Valencia et al. (2006) estimated phase variations by following the dividing lines of the olivine [$(Mg_{1-x},Fe_x)_2SiO_4$] phase diagram. Since then, considering detailed mantle mineralogy took a backseat to simpler models. But recent work have since proved the viability of new approaches.

Zeng et al. (2016) took a similar approach in using Earth's bulk mantle composition as a model for more massive planets. Their semi-empirical model is derived from the Preliminary Reference Earth Model (PREM) (Dziewonski & Anderson, 1981), a one-dimensional Earth model based off of seismological data. Specifically, Zeng et al. (2016) used the radial density profile of Earth from the PREM to model planets more massive than the Earth. Thus, they fixed the composition to that of the Earths. To scale up the Earth, they derived semi-empirical equations of state for a two layer (mantle and core) model. Below 23 GPa, they interpolated directly from the PREM data Dziewonski & Anderson (1981). In the lower mantle, at pressures greater than 23 GPa, they fit a second-order Birch-Murnaghan equation of state to the available PREM data and extrapolated beyond Earths mantle limits. They performed a similar extrapolation for the core. This model is very similar to what has already been done. It was, however, built to compare exoplanet likeness to Earth directly while varying core mass fraction, the only free parameter. They found that for Earth-like compositions, the core mass fractions of nominal rocky planets below about 5 $M_\oplus$ in mass tend to be consistent with one another, with an average value of 26 $\pm$ 7wt%.

Dorn et al. (2015) followed the same principles as the models previously discussed, in that their model is layered with a core, mantle, and H_2O regions, each of homogeneous composition. They introduce a new component in their models for rocky planets where they consider detailed mineralogical phase changes based on Gibbs free energy of possible mineral assemblages. In doing so, they could create planets of arbitrary composition based on the abundances of N, Ca, Fe, Mg, Al, and Si in a

self-consistent manner.

To find the mineralogy at depth within their planet model, they had an extra step of first assessing the possible mineral assemblages given the temperature and pressure at incremental depth. Mantle components included the following species: Na_2O, CaO, FeO, MgO, Al_2O_3, SiO_2. To compute the equilibrium mineralogy, they used a Gibbs free energy minimization package, Perple_X (Connoly, 2009) which goes through the possible assemblages to find the most likely conglomerate of mineral phases among a specific composition. Pressure was calculated assuming hydrostatic equilibrium and temperature is found by using an Earth-like geotherm. They used the thermodynamic data from Stixrude & Lithgow-Bertelloni (2005, 2011) for the mineral equations of state. The core was modeled as a pure Fe solid using an equation of state formulation from Belonoshko (2010), who fit a third-order Birch-Murnaghan equation of state up to 1000 GPa and 12000 K with synthetic data from a numerical simulation.

With the capability of modeling a continuous range of planet compositions, they used it in a unique approach to estimate exoplanet composition and the degeneracy among input parameters. They inverted their forward model with a Markov chain Monte Carlo algorithm and estimated the posterior probability distribution of the resulting composition, mass, and radius using Bayes' theorem. The Markov chain Monte Carlo (MCMC) technique is used to integrate non-analytical functions which have many components. It works by randomly selecting input parameters to get an idea of the overall distribution of results, which in this case is a probability distribution for the input parameters. Bayes' theorem essentially quantifies the probability of some event by taking the product of all relevant probability distributions. The Bayes' equation takes the following form:

$$p(\mathbf{m}|\mathbf{d}) \propto p(\mathbf{m})L(\mathbf{m}|\mathbf{d})$$

where $\mathbf{m}$ and $\mathbf{d}$ represent the sets of parameters for the model and the data. The likelihood function, $L(\mathbf{m}|\mathbf{d})$ incorporates the data available on detected exoplanets (mass, radius, and host star composition), and so represents the probability of a set of model parameters given the data and accompanying measurement errors. The priors, $p(\mathbf{m})$, are the mantle Fe/Si, Mg/Si, mantle Siwt%, and core radius. Prior distributions in this case are the probabilities of the compositional inputs. It is basically a measure of how reasonable the inputs are within the respective parameter ranges. Because Dorn et al. (2015) put no restriction on possible composition, all priors were probabilistically uniform through their ranges, except the mantle Si%, because it depends on the Fe/Si, Mg/Si values. If bulk planet compositions are equivalent to (or nearly) their host stars composition, one can place expectations on the probability of certain bulk elemental properties. To test the effectiveness of this approach, they assumed the bulk molar ratio of Fe/Si and Mg/Si mirrors the host star and they added this expectation to their likelihood function. In an alternative case, they removed this constraint.

They tested their two cases (with and without host star abundance considerations) on the solar system planets and several observed exoplanets. Their results are a probability distribution of input parameters following the MCMC inversion of their model. This is called the posterior distribution. The probabilities are a result of constraints put on their Bayes' equation with available data and range of model parameters. The resulting posterior distributions which include host star abundances are surprisingly tightly fit around the empirical values for the mantle composition and core radius of the Earth. Figure 1.7 of Dorn et al. (2015) shows the two cases. Subpanels a) through d) show the posterior distributions for the case using only the planets mass and radius, whereas subpanels e) through h) are the posterior distributions when the model included data on host star abundances in addition to mass,

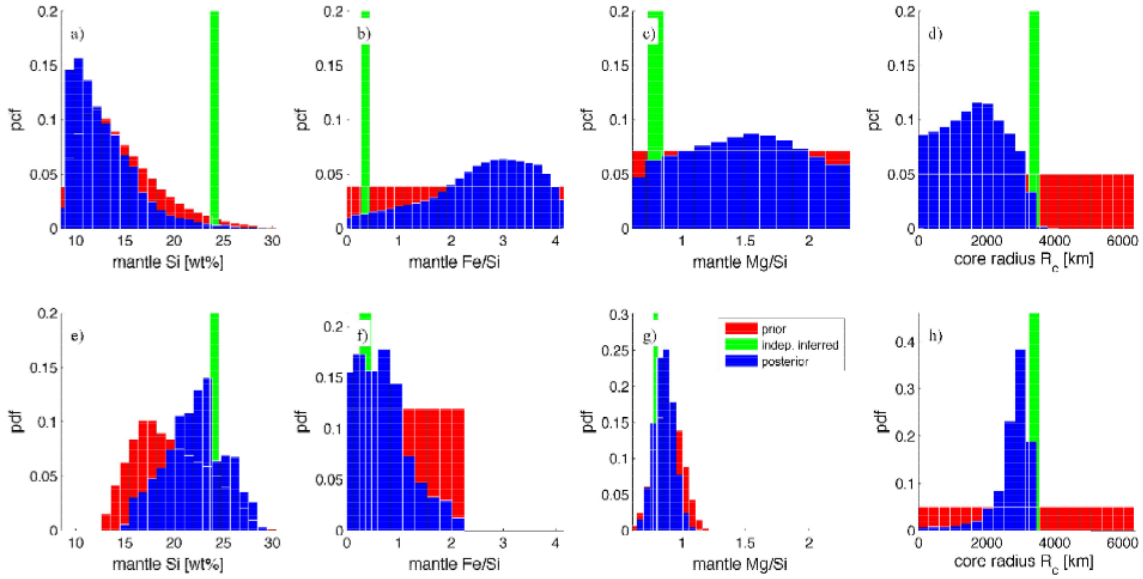

Figure 1.7

Figure 4 from Dorn et al. (2015). Posterior distributions for the Earth using two modeling cases. The distributions represent the prior (red) and posterior (blue) probability distributions for model parameters: mantle Si content, mantle Fe/Si and Mg/Si, and core radius. These posteriors are a result of using a Bayesian probability function which depends on constraints imposed by data and model parameters. a)-d) use only mass and radius in their MCMC Bayesian inversion. e)-h) use mass, radius, and host star composition as an indicator of planet composition. The latter case has a clearly more conspicuous preference towards the true values (green), indicating that host star composition can be used to asses the composition of planets.

and radius of the planet. The posteriors are clearly less ambiguous in the latter case. Using only the bulk density, as discussed earlier, offers little information on the exact mantle composition. The model is confident about the core size, but bulk density is indifferent to the Mg/Si of the mantle. On the other hand, the probability distribution for the case using host star abundances yields a strikingly accurate picture of the true composition and structure of the Earth. While these are preliminary results, they certainly are promising.

The model presented in this thesis, ExoPlex, takes inspiration from all the aforementioned models and others. We believe that modeling the details of the mineralogy for arbitrary mantle compositions is not an excessively rigorous exercise. It is informative and represents a step toward constraining the composition of planets to a level of detail that can connect planet interiors to geophysics and astrobiology holistically. Earth's interior plays an explicit role in the conditions at the surface and in the atmosphere. For example, the mantle is constantly bringing fresh, weatherable rock to the surface. Without a replenishable supply of weatherable silicates, the carbonate-silicate cycle would eventually halt Foley (2015). Understanding the mantle dynamics is key to generating a complete picture of the surface environment of exoplanets. It will be exceptionally challenging to develop a full picture of any planet. Creative techniques to adapt models to the available data as was done in Dorn et al. (2015, 2017b) and the general evolution of exoplanet models to date have shown increasing desire to reach a thorough understanding of discovered planets.

1.3 Summary

This thesis introduces a new computational tool, ExoPlex, which can be used to characterize and learn more about rocky exoplanets. The purpose of this document will be to go into full detail how our model works and to set its place among the

work discussed in this chapter. As such, the next chapter will explain the ExoPlex algorithm and the underlying physics and assumptions. We will benchmark our model against the Earth and another theoretical model. In the following chapter, several use cases will be introduced. We will also provide an exploration into the full parameter range of our model in order to define the most important observable parameters to constrain. We will also introduce the user interface provided for Python users to run ExoPlex. In the discussion, we will go into further detail on the assumptions made and the limitations of exoplanet models. The conclusion will include future work and speculation on what should be done next in order to characterize planets and eventually find out which are habitable and which are not.

Chapter 2

METHODS

2.1 Model overview

In this section we discuss the details of our code, including the algorithm, physics and underlying assumptions made. We go on to benchmark our model for rocky exoplanet with the PREM and an extrapolated version of the PREM for planets larger than Earth.

Our model is unique among those previously discussed. We follow the same assumptions in that we assume planets are spherically symmetric and so we solve equations only along the radial direction from the center to surface of planets. We pick up where the more detailed models left off by including a self-consistent treatment for mantle mineralogy. Going forward, we expand on previous work by:

- using the equation of state for liquid iron in the core
- allowing for light elements in the core (FeS, FeSi, FeO)
- making the code freely available and open source

This chapter is organized as follows. The following section will focus on ExoPlex, beginning with an overview of the input parameters in §2.2.1. In section 2.2.2, we introduce our algorithm for creating a planet model and also discuss alternative implementations of the code. We explain our treatment for modeling mineralogy and our choice in equation of state for each layer in section 2.3. Finally, we discuss the temperature profile model. We end the chapter by providing a benchmark analysis of ExoPlex.

2.2 ExoPlex

2.2.1 Model parameters

In this section, we overview the model parameters. We refer the reader to Table 2.1 for a list and short description of the parameters used in the model in addition to planet mass or radius. The coupling of bulk and core composition parameters will be explained below.

Table 2.1

List of parameters that go into the model

Parameter	Description	Default value
Composition of whole planet		
$(Si/Mg)_{bulk}$	molar ratio of Si to Mg in the bulk planet	0.91
$(Fe/Mg)_{bulk}$	molar ratio of Fe to Mg in the bulk planet	0.76
$(Ca/Mg)_{bulk}$	molar ratio of Ca to Mg in the bulk planet	0.06
$(Al/Mg)_{bulk}$	molar ratio of Al to Mg in the bulk planet	0.08
$XFeO_{mantle}$	molar ratio of Fe in FeO in the mantle, to total Fe in bulk planet	0.08
WMF	water mass fraction, fraction of planet mass that is H_2O	0.0
Composition of core		
$wtSi_{core}$	mass fraction of core that is Si	0.06
wtS_{core}	mass fraction of core that is S	0.01
wtO_{core}	mass fraction of core that is O	0.03
Boundary conditions		
$T_{surface}$	potential temperature of mantle adiabats	1000 K
$P_{surface}$	pressure at surface (Pa)	5×10^8

The composition parameters define both the internal mass distribution of each region: core, mantle, water layers. Within these regions, we assume the stoichiometry is uniform. All equations are solved assuming spherical symmetry and radial isotropy. Thus we only need to solve equations along the radial direction. To do this, we

discretize the planet into a series of concentric shells with fixed composition. Users may vary the number of shells in each region but, the default value is 1000 shells for each the core and mantle, 500 for the water layer. Below we go on to detail how we find the stoichiometry in the core and mantle using bulk composition inputs.

Composition

The essence of our model lies in its compositional dependency. Unlike the models previously discussed, ExoPlex infers the distribution of mass between the core and mantle purely from compositional inputs. This initial step is what makes our code uniquely applicable to be coupled with estimates of bulk composition.

There are two sets of composition parameters, bulk planet and core specific. Water mass fraction is defined separately and is independent of the rest of the planet. So when we speak of bulk composition, we are discussing only the refractory and metal components of the planet (core and mantle) which sits below the hydrosphere. The bulk composition is defined as relative molar abundances of Si-Fe-Ca-Al to Mg. For example $(\mathrm{Si/Mg})_{\mathrm{bulk}}$ is the molar ratio of Si to Mg in the whole planet. Additionally, we control the amount of Fe that appears in the mantle with the $\mathrm{X_{FeO,mantle}}$ parameter which indicates the fraction of total Fe moles that is present in the mantle as FeO:

$$X_{\mathrm{FeO}} = \frac{N_{\mathrm{Fe,m}}}{N_{\mathrm{Fe,m}} + N_{\mathrm{Fe,c}}}$$

, where N_X is the number of moles of some element X in the core or mantle, denoted by the subscripts c or m respectively.

In mineral physics and geology, there is a similar parameter found in the chemical compositions of silicates in which Mg and Fe are interchangeable and thus each form an endmember. The chemical formula for olivine includes a parameter x to show the fraction of fayalite ($\mathrm{Fe_2SiO_4}$) and forsterite ($\mathrm{Mg_2SiO_4}$) where the whole formula is

written as as $(Mg_{1\text{-}x},Fe_x)_2SiO_4$.

We allow for the inclusion of light elements in the core which are considered to be possible constituents in Earth's core (Birch , 1964; Anderson & Ahrens, 1994; Poirier, 1994). These include S, O and Si. They are input as a wt% of the total core mass. We neglect Ni, assuming it behaves identically to Fe. The core composition is completely described by those three inputs such that the Fe wt% in the core becomes

$$wt\%\mathrm{Fe}_{\mathrm{core}} = 100\% - wt\%\mathrm{Si}_{\mathrm{core}} + wt\%\mathrm{S}_{\mathrm{core}} + wt\%\mathrm{O}_{\mathrm{core}}$$

Before going further on how the composition inputs are convolved to calculate planet internal structure, we will explain the boundary conditions and the general algorithm.

Boundary conditions

In contrast to some like models which specify central pressure (Seager et al., 2007) we set the surface conditions and integrate inward to the center. This enables us to fix zonal mass distribution (core, mantle, water mass fractions) and solve for either mass or radius.

Surface pressure is defined as 1 bar by default but in the absence of a water layer, we use a higher pressure (on order of 10^9 Pa) because the mineralogical calculations are intended to be carried out in mantle conditions, at the same location in the planet where the potential temperature is fixed, rather than at the surface (Stixrude & Lithgow-Bertelloni, 2005, 2011).

Currently we have no treatment for a crustal layer. Earth's crust contributes a maximum of less than a percent to the overall radius. In terms of detection as an exoplanet this is well within the expected measurement accuracy for mass and radius. For modeling, the addition of a crust would have to be treated as a separate layer

which elevates the degeneracy of solutions to a level that is not necessary at this point. Additionally since all models would neglect a crust, this error is systematic and would not affect trends.

The surface temperature when there is no crust or water layer must be equal to the mantle potential temperature. This is the temperature at the top of Earth's mantle. A typical input would be on order of 1000 K. ExoPlex does allow for isothermal temperature gradients, but this likely to underestimate the temperature. While overall radius is mostly invariant to the temperature scheme (Valencia et al., 2006; Seager et al., 2007), the mineralogy calculations used are sensitive to temperature. In the case of models with a water layer, the default surface temperature is assumed to be 300 K, but the user may assume higher or lower values if desired.

2.2.2 General algorithm

Here we describe the algorithmic steps involved in passing inputs and generating a planet model based off composition and either a fixed mass or radius. More details are found below and in appendix A. The processes are carried in the following order:

1. Initialize the structure of planet based on compositional inputs (listed in Table 2.1). This step uses the composition to find an intrinsic mass distribution of the core and mantle fractions (CMF and MMF). The water layer is entered in simply as a mass fraction of the planet (WMF) and is treated separately from the core and mantle.

2. Divide the planet into concentric shells. We typically use 500 for each the core, mantle, and water layers. We assume planets are spherically symmetric and vary only along the radial direction. Concentric shells are fixed in mass and initially filled with a simple composition.

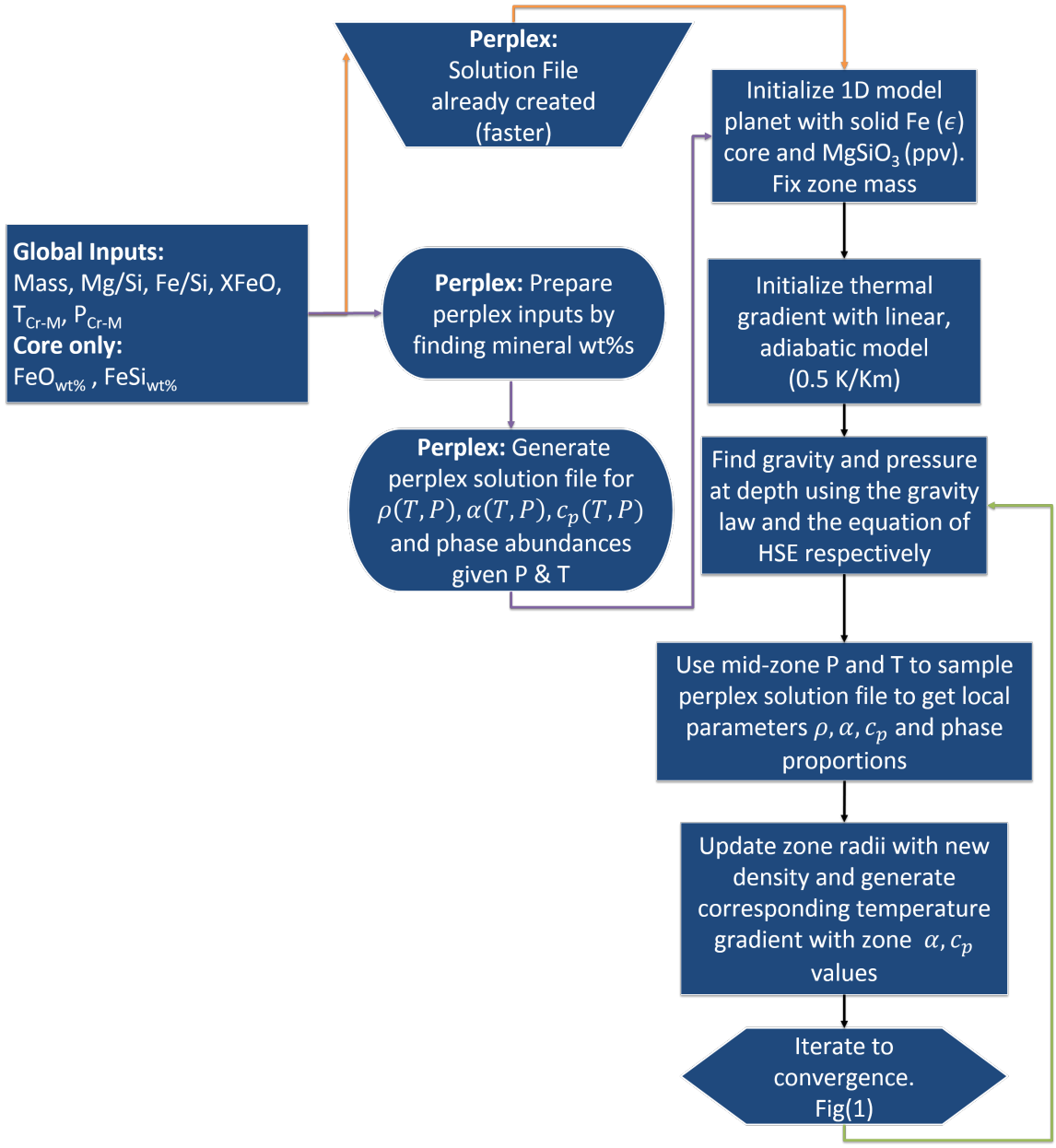

Figure 2.1

Flow chart of ExoPlex algorithm. In this chart, we show the algorithm when the code is solving for radius as a function of mass, i.e., $R(M)$. The code also can be used for the inverse problem, to find mass as a function of radius, $M(R)$.

3. Initialize the planet with the zero-pressure densities of iron (core), $MgSiO_3$ perovskite (mantle), and liquid water (hydrosphere).

4. Find the radial pressure and temperature profiles by first integrating the density to find the mass $M(r)$ enclosed within each radius r,

$$\frac{dM(r)}{dr} = 4\pi r^2 \rho(r), \tag{2.1}$$

then integrating the equation of hydrostatic equilibrium to find the pressure,

$$\frac{dP(r)}{dr} = -\frac{GM(r)}{r^2}\rho(r), \tag{2.2}$$

then assuming an adiabatic temperature gradient,

$$\frac{dT}{dP} = \frac{\alpha T}{\rho C_{\mathrm{P}}}, \tag{2.3}$$

where α, ρ and C_{P} are the expansivity, density and heat capacity of the material. We integrate equations 2.1, 2.2 and 2.3 by a discretization, using the average properties of each shell. We initialize the temperature gradient to vary linearly from the surface at 5 K/km. Following the first iteration, we use a self-consistent temperature gradient based off of mineral thermodynamic properties.

5. Update the density at each shell by using the known stoichiometry, temperature and pressure, and relevant equations of state (detailed in following sections). In the mantle, we solve the equilibrium mineralogy using Perple_X (Connoly, 2009) to produce density and other thermodynamic properties

6. After updating density in each shell, we iterate, solving equations 2.1, 2.2 and 2.3, adjusting the planet radius.

7. Iterate until convergence, defined to be when the change in density in all layers between subsequent iterations is $< 10^{-6}\,\mathrm{kg\,m^{-3}}$.

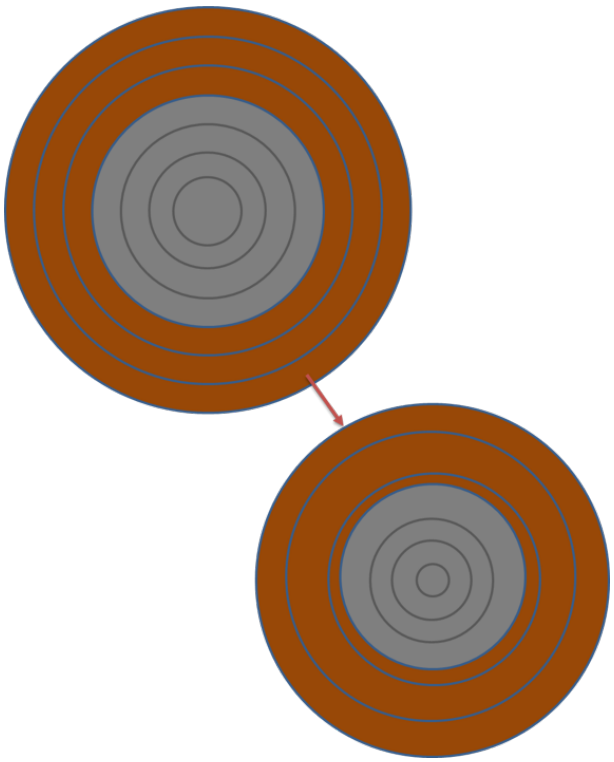

Figure 2.2

An illustration of the ExoPlex code methodology. Planets are initially divided into concentric shells of fixed mass and composition. Throughout the iterative process, the shells change in volume until the equations come into equilibrium.

An illustration of the iterative process is shown in Figure 2.2. Planets are initialized with a uniform density for each layer and then divided into concentric shells with fixed mass. Density of each shell adjusts after every iteration until the equations come into equilibrium and the planet is indeed hydrostatic. In the following section we detail how the bulk structure of modeled planets is calculated from compositional inputs.

2.2.3 Finding mass proportions of mantle and core

We define the structure of a planet purely by the input composition. This section describes our approach for finding the mass ratio between the core and mantle. The water layer is treated separately from the rock/metal portion of the planet and is controlled by entering the planet's water mass fraction; thus the remaining rocky/metal interior becomes

$$M_{\text{rocky}} = M_{\text{total}}\,(1 - \text{WMF}). \tag{2.4}$$

So, aside from the water envelope, the composition and mass of the mantle and core are convolved with the input parameters. Any change in input will alter the composition of the M_{rocky} portion whereas increasing WMF would only influence the planet's size and hence reduce interior pressure and temperature gradients. Below we explain the convolution of the composition inputs. Refer to Table 2.1 for a list of parameters.

Setting up system of equations

Our goal is to calculate the relative contribution by mass of the following oxides in the mantle: SiO_2, FeO, MgO, CaO, and Al_2O_3. The mantle mass is defined by

$$M_{\text{mantle}} = N_{\text{Fe,m}} m_{\text{Fe}} + N_{\text{Si,m}} m_{\text{Si}} + N_{\text{O,m}} m_{\text{O}} + N_{\text{S,m}} m_{\text{S}}, \tag{2.5}$$

where the variables $N_{\text{X,m}}$ are the number of moles of element X in the mantle, and m_{X} is the corresponding atomic mass. Our assumption is that these oxides completely define the mantles of rocky planets. As discussed earlier, Fe, Mg, Si, condense at similar temperatures in the solar nebula and are the dominant refractory elements in the solar photosphere. Al and Ca condense at similar, higher temperatures but are secondary in abundance (Lodders, 2003).

Similarly, we define the mass of the core from its composition. The core in our model is composed of the following components: Fe, FeS, FeO, and FeSi. The mass is found by the relationship

$$M_{\text{core}} = N_{\text{Fe,c}} m_{\text{Fe}} + N_{\text{Si,c}} m_{\text{Si}} + N_{\text{O,c}} m_{\text{O}} + N_{\text{S,c}} m_{\text{S}}. \tag{2.6}$$

Earth's core is known to have a deficit in density compared to pure Fe (Birch , 1964; Poirier, 1994; Anderson & Ahrens, 1994). There has yet to be a consensus on the proportion and composition of light alloys, but S, O, and Si are expected to be the most influential (Poirier, 1994).

To find the masses of the core and mantle, we solve a system of equations where the independent vector is the molar proportion of each elements in the core and mantle respectively:

$$\vec{x} = \begin{bmatrix} N_{\text{Fe,c}} \\ N_{\text{Si,c}} \\ N_{\text{O,c}} \\ N_{\text{S,c}} \\ N_{\text{Fe,m}} \\ N_{\text{Mg,m}} \\ N_{\text{Si,m}} \\ N_{\text{O,m}} \\ N_{\text{Ca,m}} \\ N_{\text{Al,m}} \end{bmatrix} \tag{2.7}$$

The relationship between these unknown values comes from the definitions of the input parameters: the bulk molar ratios Fe/Mg, Si/Mg, Ca/Mg and Al/Mg; the molar fraction Fe in the mantle (X_{FeO}); and the mass fractions of Si, S, and O in the core. Additional relationships come from stoichiometric arguments.

We place no direct constraint on the oxygen budget throughout the model so the relationship between the number of moles of oxygen and the relative amount of the other elements is derived from the stoichiometry of the included oxide components so that

$$N_{\mathrm{O,m}} = 2N_{\mathrm{Si,m}} + N_{\mathrm{Fe,m}} + N_{\mathrm{Mg,m}} + N_{\mathrm{Ca,m}} + \frac{3}{2}N_{\mathrm{Al,m}} \tag{2.8}$$

Each equation is listed in Appendix A, in which describe further how the vector in equation 2.7 is solved for.

2.3 Modeling mineralogy

Minerals undergo pressure-induced phase changes. These are alterations to the crystal structure of atoms within a mineral. These deviations will alter not only density but also how a mineral behaves thermodynamically. To differentiate planets of different composition but similar overall density, we utilize this property of materials. Our treatments for modeling the mineralogy of each composition region differ, as explained below.

2.3.1 Core

While the core is much simpler than the mantle compositionally, there is more uncertainty in describing materials at core pressures and temperatures. There are also fewer elements in Earth's core that can have a significant impact on thermodynamic characteristics, as compared to the mantle. Despite this, the current understanding of the exact composition of the core is incomplete (Poirier, 1994). In our treatment we try to remain as accurate as possible by not extrapolating too far beyond what is empirically understood about core minerals at extreme conditions. Below we discuss our treatment for modeling cores, beginning with the allowed composition.

Core light elements

Earth's core is predominantly, but not entirely, iron and nickel. It is well known that there exists a density deficit in Earth's core that points to the existence of some mass fraction of light alloying elements (e.g. Birch (1964); Anderson & Ahrens (1994); Poirier (1994)). Accounting for roughly a 10% density deficit for the Earth's core, these light alloys cannot be neglected when modeling exoplanets in other systems. While the detectability of core composition in exoplanets is slim and may never be possible, the density deficit caused by non-pure Fe cores can impact core size and state, and in turn geophysical processes. Leaving the possibility of non-singular core composition elevates degeneracy in the solution, but it is better to leave the model open to the plethora of probable scenarios. Our consideration of non-singular core compositions is unique among exoplanet models.

The light element content of Earth's core is still debated and arguments for S, Si, O or some combination of the three are credible (Birch , 1964; Poirier, 1994). While other components likely exist in Earth's core—including H, Ni, and Cr as suggested by McDonough (2003) and others—Si, S, and O more than likely dominate in both presence and impact on the core size. Ni can possibly be the most abundant non-Fe component of the core; however its similarity to Fe in density and chemical properties leaves it impossible to even infer.

The mineralogical system used in our model is simple in comparison to the mantle; it is an assemblage of pure Fe, FeS, FeSi and FeO. The major drawback is that equations of state and polymorphs of these components at core conditions are less well known compared to minerals at more moderate conditions. This is especially true for the iron alloys.

To avoid ambiguity, we take the best defined and prevalent material, pure Fe

and allow the alloys to manifest through a deficit of the reference density used in the equation of state, ρ_0. For Earth's core, light elements effectively lower the molar mass of the core but show almost no perturbation to compressibility. Anderson & Ahrens (1994) found that the bulk moduli predicted by their equation of state formulation for pure liquid Fe agrees well with the PREM (Dziewonski & Anderson, 1981). That is, without knowing the composition of Earth's core, we can model the density at depth as long as we know the pressure, temperature, and ρ_0. We extend this finding to arbitrary abundance of the included light elements.

To influence the molar mass of the core medium, we calculate the average molar mass, $\bar{M}_{core}$ of Fe and its lighter alloys using the inputs for mass fraction of S, Si, O. So then a greater input of $\mathrm{wtO_{core}}$ for example, raises the total contribution of FeO to the core; which brings down the molar mass and initial density used in the equation of state.

We find the total number of moles in the core of each component, $N_{\mathrm{core}} = \sum_i N_{X_i}$ where X_i = Fe, Si, S or O. To do this, we convolve the inputs from Table 2.1 which results in the N_{X_i} (detailed in Appendix A) for the core and mantle. We then calculate the molar fraction of each element in the core

$$x_i = N_{X_i}/N_{\mathrm{core}}$$

We add up the contributions to the core mass from each component to find an average molar mass:

$$\bar{M}_{\mathrm{core}} = \sum_i x_i * m_{X_i}$$

, where m_{X_i} is the molar mass of element X_i. We use this average molar mass in the equation of state below to reflect the density deficit caused by light alloys.

Core equation of state

We elect to use liquid Fe as our principal core state, unlike the general convention of similar models (Seager et al., 2007; Zeng & Sasselov, 2013; Dorn et al., 2015, 2017b). However, this approach is not entirely unique: Valencia et al. (2006) allowed for liquid Fe in their core. Earth's core is predominantly in the liquid phase: the solid portion of the core accounts for just 5% of the core by mass (Yoder, 1995). Using a liquid iron equation of state is therefore preferable, but it has been pointed out by Unterborn et al. (2016) that models of the Earth using only the liquid core state systematically underestimate radii. While liquid-solid state changes can be modeled, it was shown by Valencia et al. (2006, 2007a) that modeling geotherms of other planets is difficult task and comes with little benefit. They also showed that liquid cores may be ubiquitous among super-Earth sized planets. It is then more consistent empirically and theoretically to assume a 100% liquid phase.

Our equation of state comes from Anderson & Ahrens (1994). They provide an empirical fit of liquid iron to a second-order Birch-Murnaghan equation of state (BM2) centered at 1 bar and 1811 K. The parameters used are as follows: density, $\rho_0 = 7019$ kg/m^3; isentropic bulk modulus, $K_{S0} = 109.7$ GPa; first pressure derivative of K_S, $K'_{S0} = 4.66$; and the second pressure derivative of K_S, $K''_{S0} = -0.043$ GPa^{-1}.

2.3.2 Mantle

To find the stable phases of mineral assemblages at depth, we utilize the Gibbs free energy minimization package, Perple_X (Connoly, 2009). Our mantle model is composed of the following oxides: SiO_2, FeO, MgO, CaO, and Al_2O_3. The minimization scheme uses the input composition to probe a list of known mineral endmembers to find the most likely phases present at a certain temperature and pressure. The

result is an assemblage of the thermodynamically consistent phases and its physical properties (e.g. density, heat capacity).

The formulation used for the physical parameter calculations comes from Stixrude & Lithgow-Bertelloni (2005, 2011). They also provide the full list of minerals included. To calculate thermodynamic properties, they relate all thermal parameters to the Gibbs free energy parameter, G. This is done through a series of derivations of G which is possible because G is related to minerals through their thermodynamic properties.

Density is found by using a third-order Birch-Murnaghan equation of state (BM3) where parameters are dependent on the specific mineral assemblage at a given pressure and temperature. In this way, calculations are thermodynamically self-consistent. See Stixrude & Lithgow-Bertelloni (2005, 2011) for equation of state (EOS) parameters.

It is important to note that EOS data for these materials were originally motivated by understanding Earth's interior. Using these methods for conditions which exceed those in Earth's lower mantle (e.g. in super-Earths) is beyond the scope of previous works and results in an unavoidable extrapolation. All models suffer from this shortcoming when analyzing super-Earths or Earth mass planets with small cores. Perple_X was built to handle a variety of compositions so we are confident in the mineralogical results from the Gibbs minimization. We do take steps to ensure the most accurate solution attainable by splitting the upper and lower mantle calculations.

Upper and lower mantle

Earth's mantle spans a range in pressure up to 136 GPa. The upper mantle contains a complex mixture of end-member mineral phases, whereas the lower mantle is relatively simple on a whole. Phase transitions occur more rapidly along a shallow pressure gradient than they do at the high pressures of the lower mantle. It can be seen

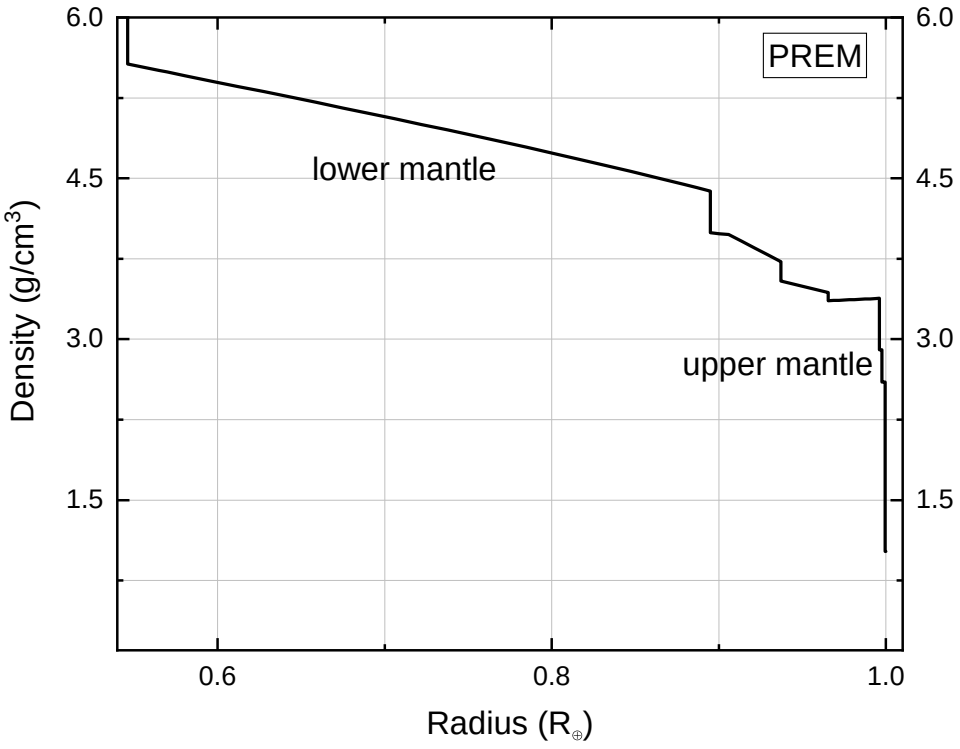

Figure 2.3

Radial density profile of Earth's mantle in the Preliminary Reference Earth Model (Dziewonski & Anderson, 1981). The lower mantle is distinctly uniform in mineralogy compared to the upper mantle. Density jumps are a result of mineral phase transitions.

in Earth's seismological density profile in figure 2.3 that the rapid rise in density at shallow depth is caused by phase transformations into denser polymorphs. The phase changes are conspicuous as they almost appear to be vertical steps in density, monotonically increasing with depth. In the same figure, it can be seen that after a certain depth, the density profile is smooth. Below a depth of about 660 km, the mineralogy seen in the mantle simplifies, due to a marked change in phase of mostly ringwoodite to periclase and bridgmanite. This is where the lower mantle begins, as annotated in Figure 2.3. For a given composition, one can expect to see some combination of only periclase, stishovite and bridgmanite below this depth for an Earth-mass planet. At even further depths, the post-perovskite phase of $(Mg_{1-x},Fe_x)SiO_3$ exists. In planets more massive than earth, it is this phase which is expected to dominate mantles.

This apparent simplification in phases leads us to delineate the lower and upper mantle phase equilibria calculations. Phase transitions are most sensitive to pressure changes along a given temperature gradient, so we select a sufficiently high pressure cutoff point of 125 GPa. Below this pressure (at shallower depths), we use Perple_X to its full power, allowing for it to test the stability of all possible phases within the desired composition at high resolution (small ΔT, ΔP grid). At greater depths, we use a lower-resolution grid and simplify the phase space only to those phases which are likely to be present. We do this to expedite calculations and allow for higher resolution only where the mineralogy is more diverse.

While the lower mantle conditions result in simpler calculations with fewer end-members, we do recognize that this is the region where extrapolation of parameters is most necessary. The calculation of certain thermoelastic properties therefore becomes less trustworthy as models move beyond Earth-like conditions, especially to higher pressures. However, the included high-pressure polymorphs of pyroxene, olivine and quartz are the densest known to occur in Earth, as the smoother density gradient

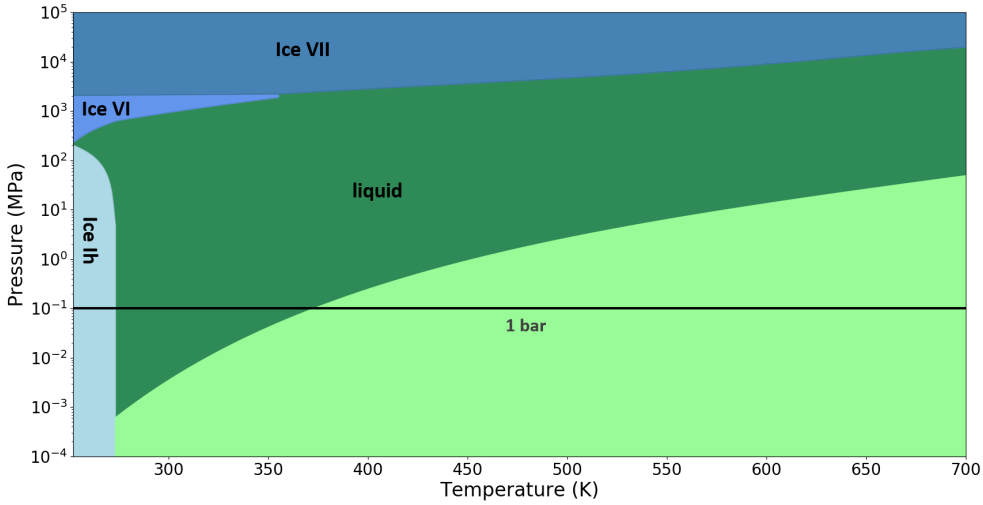

Figure 2.4

Modified water phase diagram used in ExoPlex. We use the boundaries between phases to find the state of water at certain pressure and temperature combinations.

in the lower mantle indicates. Modeling rocky-type planets much more massive than the Earth probably will not include even higher pressure phases. Thus, in terms of density, the deviation would not be significant enough to detect in the overall mass or radius. In our one-dimensional model, these phase changes would be expected to occur in a deep interior shell which holds less volume than shallower shells, and is thus less impactful on the total mass and radius.

2.3.3 Water layer

We include a water layer that sits on top of the rocky layers. With a much lower density, this layer is most influential on the detected radius of exoplanets. For consistency we include liquid and solid states of H_2O. These include high-pressure Ice VI and VII. The water phase diagram below $\approx$ 270 K shows several minor phases of ice, namely ice II, V, and III. We choose to neglect these phases in favor of a more

Table 2.2

Equation of state parameters for H_2O phases

Phase	ρ_0 (g cm^{-3})	K_0 (GPa)	K_0'	EOS	References
liquid	1	2.06	6.29	BMIV	1
ice Ih	0.91672	9.2	5.5	BMIII	1
ice VI	1.2714	14.01	4	BMII	2
ice VII	1.4424	20.15	4	BMII	2

1 International Association for the Properties of Water and Streams; 2 Bezacier et al. (2014)

simplified phase diagram by limiting the minimum surface temperature in our model to 300 K. Below this temperature, the model will still calculate phase boundaries and densities, but minor phases will not be included. Our phase diagram for H_2O appears in Figure 2.4. The thermodynamic parameters and equations of state used for each phase are listed in Table 2.2.

2.3.4 Temperature profile

It has been shown by other groups that internal temperature has little significant contribution to density and thus overall mass and radius (e.g. Valencia et al. (2006); Seager et al. (2007). This and the current high-pressure data on terrestrial minerals led many early models to consider only "cold planets," i.e., those which are internally isothermal at some low temperature, typically 300 K Valencia et al. (2006); Seager et al. (2007); Zeng & Sasselov (2013). These models were effective for planets of uniform mineralogy and with no water layer. To understand detailed mineralogy for a variety of planet compositions and properly include a water envelope, it is necessary to incorporate some internal geotherm profile where temperature increases with depth,

as in Earth's interior.

We use an adiabatic temperature gradient which represents Earth's temperature profile without the contribution from radiogenic heating. This takes the form

$$\frac{dT}{dr} = \frac{T\alpha g}{c_{\mathrm{p}}}, \tag{2.9}$$

where the thermal expansivity (α) and heat capacity (c_p) depend on the equilibrium mineralogy at depth. We integrate this equation from the near-surface using the potential temperature.

An adiabatic profile can be assumed for a well-mixed, convecting mantle. Earth's true temperature gradient is hotter in the mantle than the adiabatic profile. This is likely due to radiogenic heating, which reduces the viscosity (ν) of the mantle. A reduced viscosity is thought to contribute to enhancement of convective heat transport in some regions of the mantle. The vigor of convection is proportional to a power of the Rayleigh number Ra, which is inversely proportional to the viscosity ν: Ra $\propto \nu^{-1}$. Reducing the viscosity raises the chance of convection for a fixed temperature gradient (Foley, 2015).

We extend our adiabatic temperature gradient into the core in our model. Our treatment of core composition does not invoke a calculation of stable phase assemblage as we use for the mantle. This makes density the only parameter which we calculate for in the core, which is invariant to temperature profile. This decouples the calculation of density and temperature in the core, unlike the case for the mantle. Our core model is composed of liquid Fe which is likely to convect; however we note this has no contribution to a static planetary model. In a more rigorous model, this will have to be altered to consider the various modes of heat transport, namely convection if we are to consider dynamic planets as in Valencia et al. (2007a).

Chapter 3

RESULTS

3.1 Tests

3.1.1 Computational time

We begin by testing the level of detail necessary to accurately model mantles. As discussed in a previous section, we use Perple_X to calculate the equilibrium mineralogy in the mantle. To do this, we convolve the composition inputs to find the mass proportion of the following mantle components: SiO_2, MgO, FeO, CaO, and Al_2O_3.

Neglecting a partitioned crust, we assume that the mantle is of uniform composition, with relevant mineral phase transitions dependent on pressure and temperature. We pass these values to the Perple_X code, which performs a Gibbs free energy minimization technique that finds the stable phases and their thermodynamic parameters for a range of pressures and temperatures. Perple_X outputs a discrete grid of density, bulk modulus, heat capacity etc., with sample spacing dependent upon the number of samples desired and the range of temperature and pressure calculated. For example, a typical range of expected mantle temperatures is between 300 and 3000 K and the accompanying range of pressure is 1 to 200 GPa. We linearly sample the combination of temperatures and pressures with some chosen grid size. For a 10 x 10 spacing, we will sample in total 100 temperature and pressure pairs. We can enhance the level of detail in our mantles by increasing the grid size which in turn reduces the spacing between each sample. Doing so, however, comes at the cost of higher computational time. If the resolution is too low, interesting phase boundaries are lost and the overall

result will be inaccurate. To test the latter of these consequences, we compare the results of high-, mid-, and low-resolution models.

Table 3.1

Temperature and pressure grid spacings for low, medium and high resolution cases

Resolution	Δ Pressure (bar)	Δ Temperature (K)
Lower mantle		
Low	725,000	550
Medium	214,666.7	183.3
High	80,555.6	61.1
Upper mantle		
Low	124,500.1	350
Medium	41,500.0	116.6
High	13,833.3	38.9

Figure 3.1 shows a radial density distribution for the mantle of a 1 $M_{\oplus}$ planet with a bulk composition similar to Earth's. The upper mantle phase transformations are revealed through density jumps. Each curve represents a different spacing of temperature and pressure in the perple_x solution file that ExoPlex samples from to find local termodynamic parameters int he mantle. The spacing corresponding to each resolution in figure 3.1 are shown in table 3.1. The green curve has the highest resolution (smallest spacing between P and T samples); here all of the important transitions are clearly represented. These transitions are hardly visible for the lowest resolution case. Taking the highest resolution case to be the most accurate, the deviation of the overall radius for the lowest resolution model is less than one tenth of a percent, while the computation time required is an order of magnitude longer for the

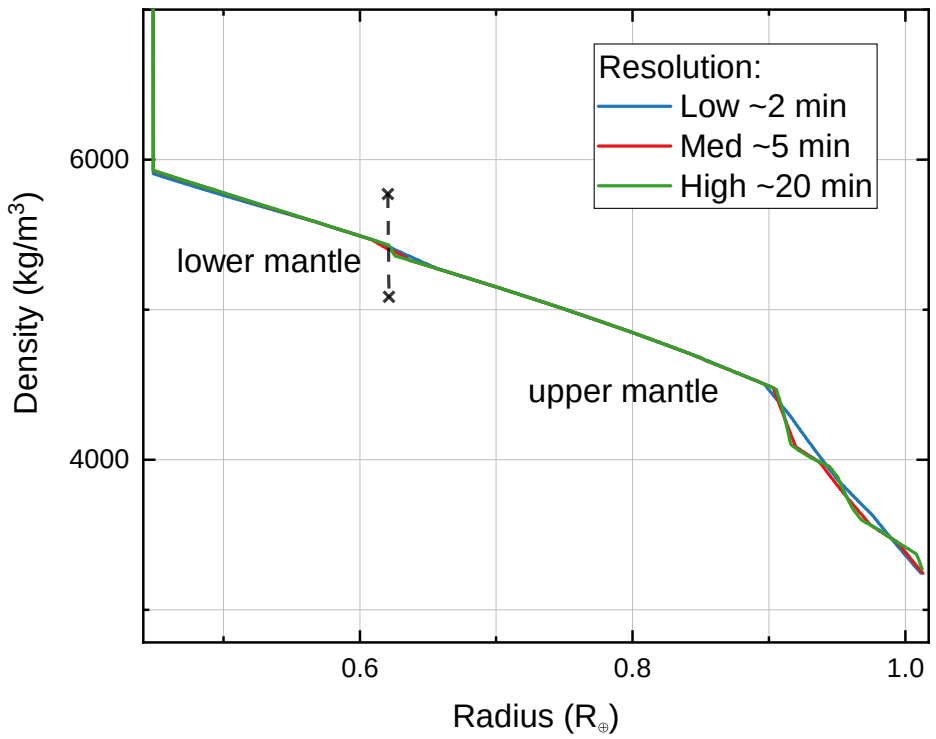

Figure 3.1

Density vs. radius inside a 1 $M_\oplus$ planet in the upper mantle, including the transition zone, for the low-, medium-, and high-resolution models (computational times are listed for each case). The lowest resolution uses too coarse a grid to fully capture all the mineralogical transitions of the transition zone, but yields almost the same radius of the planet.

high resolution compared to that of the lowest. We therefore favor the low-resolution case using 10 x 10 spacing in most cases, because of the lower computational time and the marginal benefits of modeling the mineralogy at high resolution. To fully capture the mineralogical transitions in the transition zone, the medium-resolution grid is sufficient.

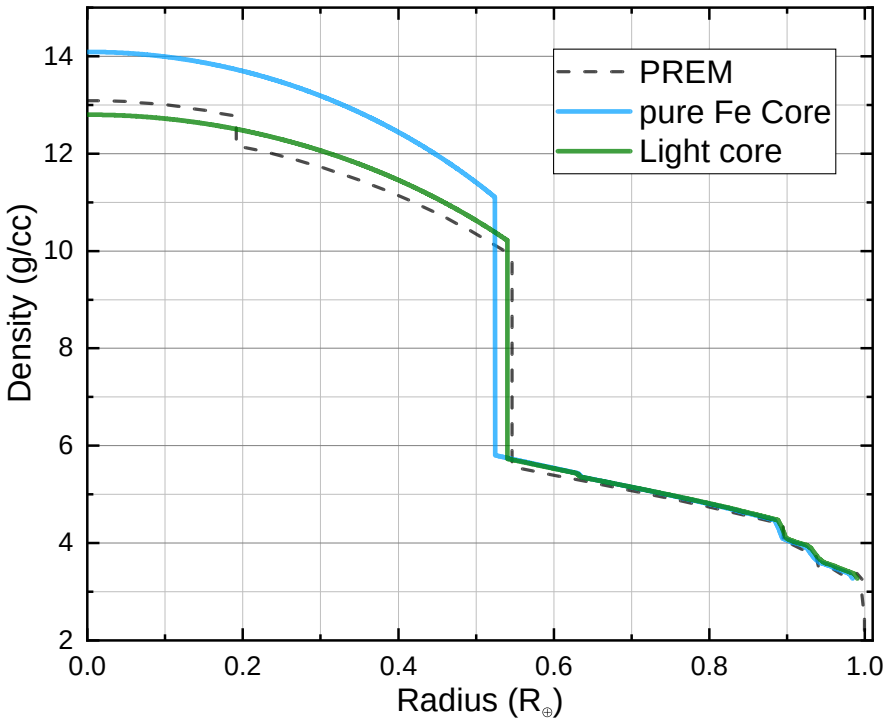

Figure 3.2

Best ExoPlex model for Earth using composition parameters from McDonough (2003) as listed in Table 3.2. The light blue and green curves are ExoPlex models with Earth-like mantles. The blue curve has a pure Fe core, whereas the green curve includes core impurities that reduce its density. These are compared with the empirical model of Earth (PREM), given by the black dashed line.

3.2 Benchmarking

3.2.1 Empirical Earth model

As a baseline, we compare our model with an empirical model of the Earth. We use the Preliminary Reference Earth Model (PREM) (Dziewonski & Anderson,

1981) as our comparison empirical model. The Earth offers our only opportunity to empirically test the our upper mantle mineralogy model used. Figure 3.2 shows the radial density profile for PREM and our best Earth model. We use the McDonough (2003) compositional model for the Earth and fix the core to 32.3% of Earth's mass (Yoder 1995). The fiducial Earth composition used is summarized in Table 3.2. Two model curves are shown. The blue curve shows a model with a pure iron core whereas the green curve corresponds to a core of 92.1%Fe, 6.0% Si, and 1.9% S. Both models produce radii that would match 1 Earth radius to well within observation noise for the transit method, indicating that light alloying elements in the core of an exoplanet would not be detectable using mass and radius. With lighter alloying elements are in the core, total radius is $R_{alloy} = 0.9901\ R_\oplus$ whereas with a pure Fe core, $R_{noalloy} = 0.984\ R_\oplus$. Nonetheless, light alloying elements in the core matter for the internal structure of the planet. We consider the match between the ExoPlex model and PREM to be very satisfactory.

3.2.2 Other theoretical models

For planets larger than Earth, we compare our model with the semi-empirical model of Zeng et al. (2016). In Figure 3.3, we plot the radius of an exoplanet vs. its mass, for masses between 0.1 and 5 $M_\oplus$, as predicted by the ExoPlex model. The parameters in Table 3.2 are assumed, with the exception of mass and core mass fraction (CMF), which are allowed to vary. On average, the curves deviate from one another by less than 1%. For models which have a mantle, ExoPlex radii are systematically smaller than the equivalent Zeng et al. (2016) models. Clearly this discrepancy is rooted in how we model the mantle. Interestingly, Zeng et al. (2016) report a 1% error in upper and lower mantle models by not considering detailed phase transformations. Because $R \propto \rho^{-1/3}$, a systematic discrepancy in density will have

Table 3.2

ExoPlex parameters for our fiducial Earth model.

Parameter	Value	ref.
Mass	1 $M_\oplus$	1
CMF	0.323	1
$(Fe/Mg)_{mantle}$	0.12121	2
$(Si/Mg)_{mantle}$	0.79798	2
$(Ca/Mg)_{mantle}$	0.06566	2
$(Al/Mg)_{mantle}$	0.09091	2
$wtSi_{core}$	0.06	2
wtS_{core}	0.019	2
wtO_{core}	0.0	2

[1] Yoder (1995) [2] McDonough (2003)

little influence on radius unless mass is significantly higher. Figure 3.3 shows exactly this. At low masses, the models are identical whereas they assume slightly more divergent trajectories as mass increases. Overall, the two models are in agreement but it is interesting to see how the known discrepancy can be caught using a more rigorous model for mantle mineralogy. As for the core, our model matches the Zeng et al. (2016) results well for the 50% and 100% core mass fraction cases in contrast to the cases with a lower CMF, indicating agreement for at least the core models.

3.3 Characterizing rocky planets

3.3.1 Models utilizing mass and radius data only

We have so far explained our model as one which can utilize data on host star composition as an aid to ultimately understanding the internal structure of rocky

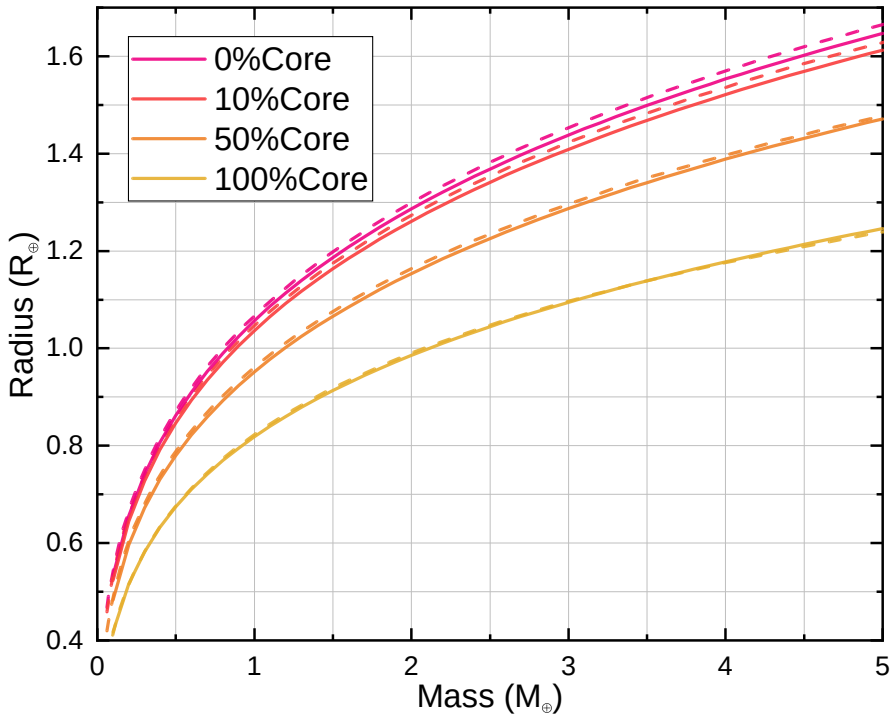

Figure 3.3

Mass-radius relationship for rocky exoplanets with various core mass fractions, as predicted by ExoPlex (solid lines) and equivalent models from Zeng et al. (2016) (dashed lines)

planets at a new level of detail. However, a first-order analysis is at once interesting to give an idea of the degeneracy of model results for a specific mass and radius. We illustrate our ability to model planets from measurements of only their mass and radius through ternary diagrams. Figure 3.4 shows a ternary diagram where the sides represent fraction of core, mantle, and water by mass (CMF,MMF,WMF). (The sum of these three quantities is 1.) In this example, the core is set to pure Fe, the mantle is Earth-like (mantle composition outlined in Table 3.2), and the H_2O layer

sits above the core and mantle; it is composed of liquid water and high-pressure ices (determined using the modified phase diagram in Figure 2.4). The contours represent curves of constant radii of $0.85, 0.90, ...1.15\,R_\oplus$ for a 1 $M_\oplus$ planet. It is assumed that an exoplanet might be observed to have a radius of $1\,R_\oplus$, with a 1σ uncertainty of $\pm 0.05\,R_\oplus$; these contours illustrate how the uncertainty in radius would translate into uncertainty in composition. The dotted line in this figure represents a constant bulk planet molar ratio of Si to Fe of 0.6, which was likely the composition of the solar nebula the Earth formed in. Regions in the ternary diagram below this line would correspond to enhancements of Fe, possibly from impacts having partially stripped the mantle. Regions above this line might correspond to planets formed in highly oxidizing environments where a higher fraction of available iron might reside in the mantle (Valencia et al., 2007a).

From inspection of Figure 3.4, a 1 $R_\oplus$ planet whose radius could be in the range $1\pm 0.15\,R_\oplus$ could be consistent with the entire range of mantle mass fraction (MMF) from 0 to 100%, and core mass fractions between 0 and 95%. If the radius were constrained to $1\pm 0.05\,R_\oplus$, not much more is constrained: mantle fractions between 0 and 95%, and core mass fractions between 5 and 85% are allowed. With the typical observational uncertainties in radius, mass and radius alone do not significantly constrain core and mantle mass fractions. The mass and radius are better able to constrain water mass fraction. If the radius is constrained to the range $1 \pm 0.15\,R_\oplus$, the allowed water mass fraction lies between 0 and 50%, and if the radius is constrained to the range $1\pm 0.05\,R_\oplus$, the allowed water mass fraction lies between 0 and 30%. Of course, not all of these compositions are realistic. For instance, a 1 $R_\oplus$ can be made with 75% core mass fraction and the rest water. Noting the differences in condensation temperature of silicates and iron bearing minerals and the relative similarity in abundance of Si and Fe in the universe, it is unlikely to form such a massive planet without a core.

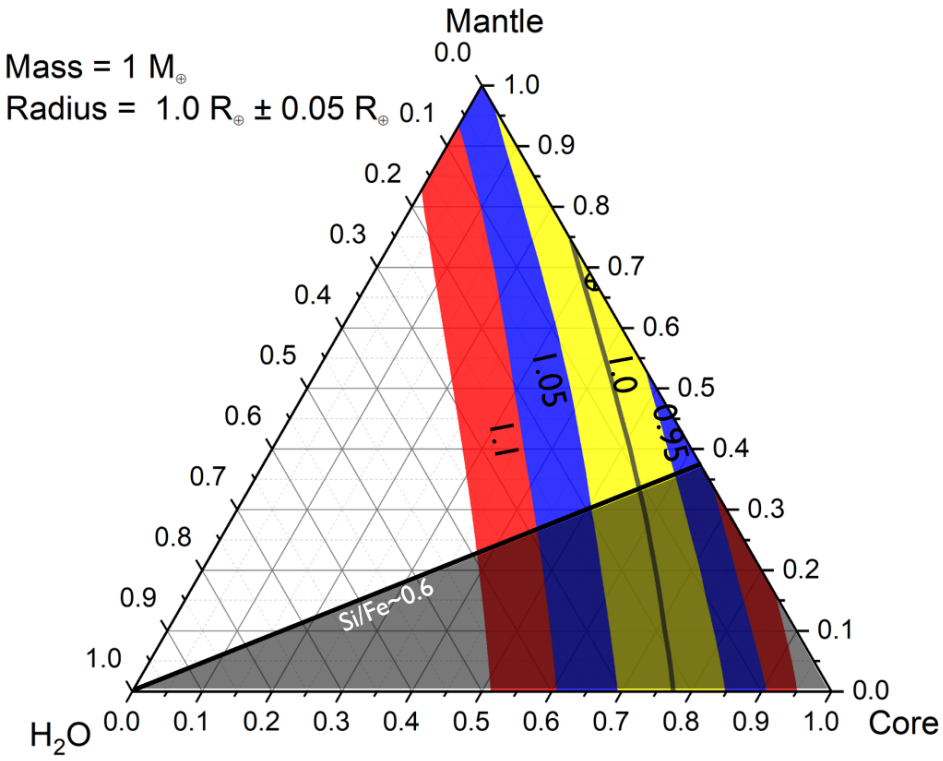

Figure 3.4

Ternary diagram with the right side representing the mass fraction of the planet that is mantle, the bottom side representing the core mass fraction, and the left side representing the mass fraction of water layers. Mass is fixed at 1 $M_\oplus$. Bands represent combinations of paramters yielding a radius within 3 σ of 1 $R_\oplus$, where a 1σ uncertainty in R is $\pm$0.05 $R_\oplus$.

In addition, while the sensitivity of results to water content is more significant, given the likely uncertainties it would be difficult to distinguish between planets bearing an Earth-like abundance of water or worlds entirely covered in deep oceans and no land mass.

Figure 3.5 shows a similar ternary diagram for a hypothetical planet with a mea-

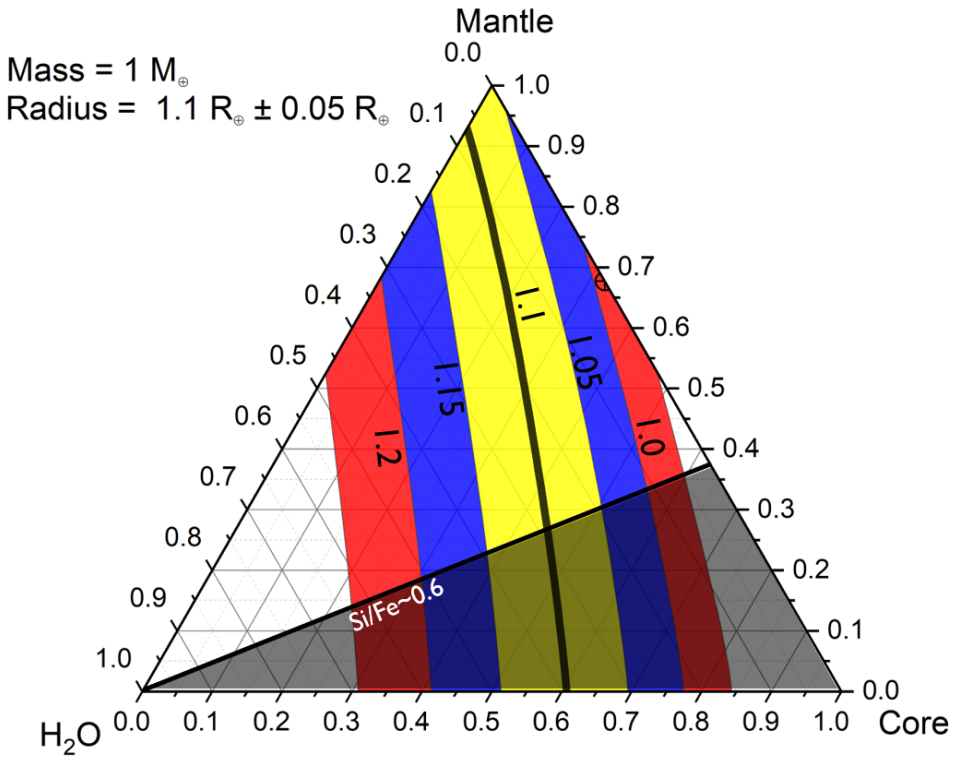

Figure 3.5

Ternary diagram with sides representing the mass fraction of core, mantle, and water layers. Mass is fixed at 1 $M_\oplus$. Bands represent locations where the radius is within 3 σ of 1.1 $R_\oplus$ $\pm$0.05 $R_\oplus$.

sured mass of 1 $M_\oplus$ and radius of 1.1 $R_\oplus$ $\pm$0.05 $R_\oplus$. A 10% increase in radius while fixing the mass results in a 25% reduction to overall density. With this, the ambiguity in the possibly solutions for internal mass distributions is enhanced. Lower density planets are more difficult to constrain because it becomes more likely that lighter planets contain some quantity of water. If the radius is constrained to the range $1 \pm 0.15\, R_\oplus$, the allowed mantle fractions are 0 to 100%, the allowed core mass fractions are 0 to 85%, and the allowed water mass fractions are 0 to 70%. If the radius is

constrained to the range $1 \pm 0.05\, R_{\oplus}$, the allowed mantle fractions are 0 to 100%, the allowed core mass fractions are 0 to 70%, and the allowed water mass fractions are 0 to 50%. The only chance to reduce the degeneracy using simple arguments, realizing that some solutions are unrealistic. The ternary diagram shows that planets with no core and thus a mixture of only mantle rock and H_2O are a good fit to the mass and radius; but this scenario would be unlikely, given that Si and Fe tend to exist in comparable quantities for stars measured thus far (Hinkel et al., 2014). This, coupled with the constraint that the Si/Fe fraction should be roughly preserved throughout planetary accretion due to similar condensation temperatures, may slightly alleviate the degeneracy of solutions.

Generally it is not possible to constrain the bulk composition of a rocky exoplanet using only its mass and radius measurements. The situation worsens when considering lower-density planets that require some fraction of water in their solutions. The problem lies in the lack of available data compared to the desired solutions. We have two data points (mass and radius) and at least three dependent variables (CMF, MMF, WMF). Using compositional arguments (like the suggestion that the host star silicon and iron abundances should be similar to the planetary abundances) will be necessary in future planetary characterization efforts. We have designed ExoPlex with this in mind. The following section will detail how our code is used as a Python library or standalone set of scripts.

3.3.2 Models using additional data to constrain composition

Figures 3.6 and 3.7 illustrate how mass-radius diagrams can be used in conjunction with stellar data to constrain planetary composition and internal structure. Figure 3.6 shows the mass-radius relationship for planets up to 5 $M_{\oplus}$, for compositions that are 100% core, or 100% rocky mantle. Si/Mg and other ratios are fixed to the Earth

values. For a 5 $M_\oplus$ planet, radii could range from 1.24 to 1.65 $R_\oplus$. An observed exoplanet would have to lie outside this large rage to be determined to have a composition other than rock and metal, e.g., bearing significant water. The shaded region in between shows the curves that have Fe/Mg within the range of stellar compositions in the Hypatia catalog. The dashed curve denotes those values with the mean ratio of the 446 stars in the Hypatia catalog with known planets, Fe/Mg = 0.76. The dark shaded region uses Fe/Mg values within $1\sigma = \pm 0.15$ of this value, and the light shaded region includes curves across the entire range of Fe/Mg values in the Hypatia catalog stars with planets. Core and mantle mass fractions outside the values corresponding to these shaded regions must be considered highly improbable. With that consideration, a 5 $M_\oplus$ planet with radius outside the much smaller range 1.50 to 1.60 $R_\oplus$ could be considered to incorporate other species such as water. Intriguingly, there is no evidence that Kepler-78b, Kepler-10b, or Kepler-36b (or Mars, Venus or Earth) have unusual Fe/Mg ratios or significant quantities of materials other than rock and metal. In contrast, Trappist-1b probably does contain signficant water.

Figure 3.7 shows a similar mass-radius diagram for planets up to $5M_\oplus$, except Fe/Mg is fixed to the terrestrial value, and Si/Mg is varied across the range seen in the planet-hosting stars in the Hypatia catalog. The shaded region shows the curves across the entire range of the Si/Mg ratio among such stars, roughly 0.91 ± 0.16. The predicted radius of the planet is not sensitive to the Mg/Si ratio. There is no evidence that Kepler-78b, Kepler-10b, or Kepler-36b (or Mars, Venus or Earth) have unusual Si/Mg ratios or significant water, but Trappist-1b probably does.

3.4 Using ExoPlex

Our primary goal was to create an open source code that models exoplanets based on their mass, radius, and composition. To this end, we have developed an intuitive

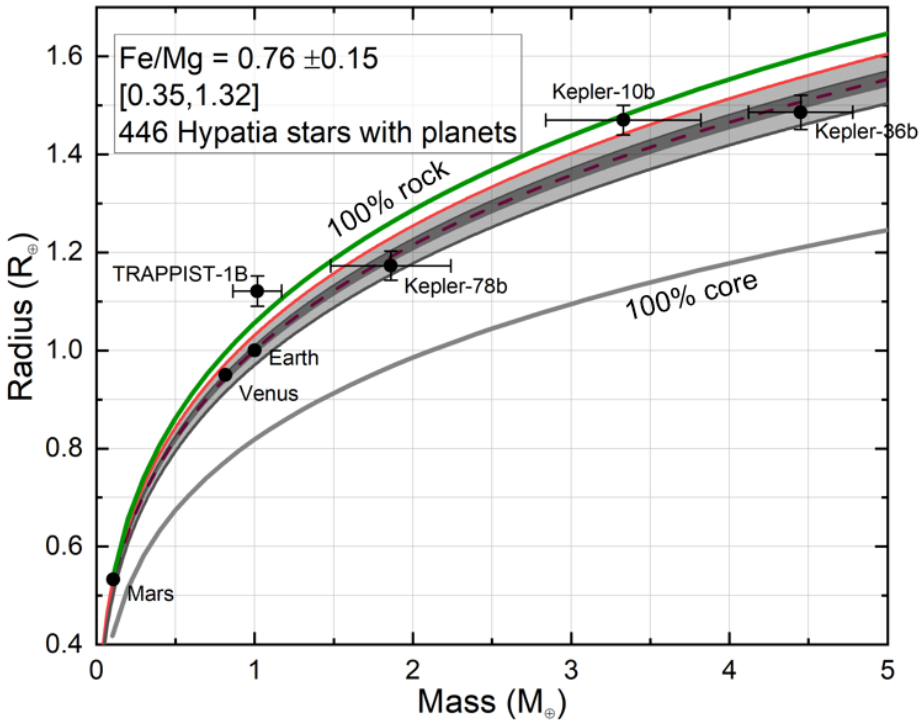

Figure 3.6

Mass vs radius diagram for planets up to 5 M⊕. Planet composition is fixed to the canonical Earth values while bulk Fe/Mg is varied between the minimum and maximum values found in the Hypatia catalog. The shaded region represents the range of radii possible for the extreme Fe/Mg values whereas the darker shaded region is the mean Fe/Mg value (pink dotted line) within 1 σ.

user interface which takes the form of functions that can be called into user's codes from either a local install of ExoPlex from GitHub or by using ExoPlex as a Python library. Currently ExoPlex can be run on Linux and MAC OS operating systems. To use as a library, ExoPlex may be installed from the Python Package Index (PyPI) using pip with the following command line function:

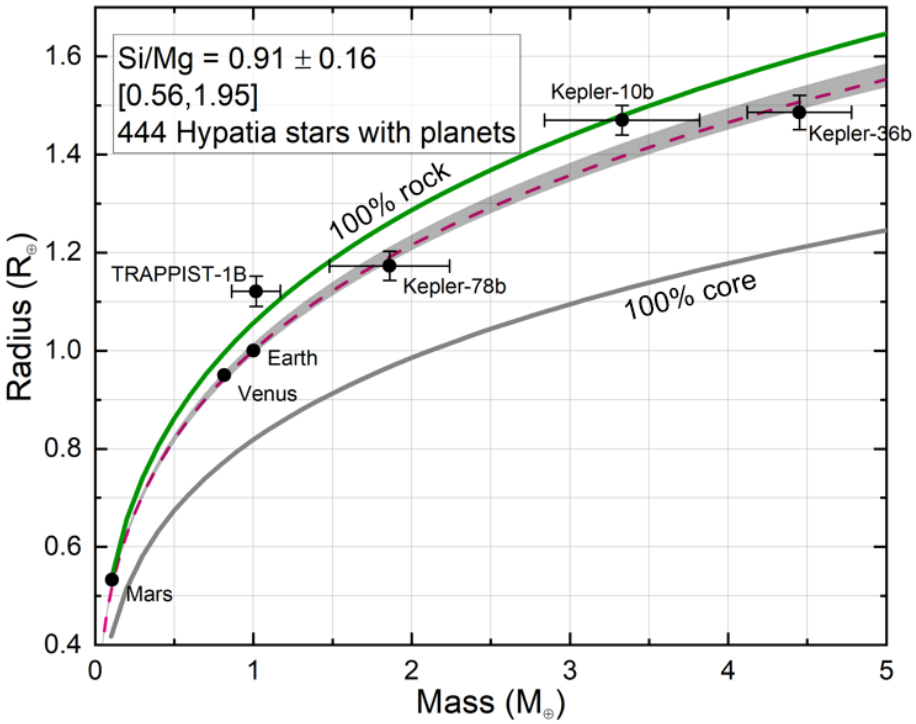

Figure 3.7

Mass vs radius diagram for planets up to 5 M⊕. Planet composition is fixed to the canonical Earth values while bulk Si/Mg is varied between the minimum and maximum values found in the Hypatia catalog for stars with known planets. The shaded region represents the range of radii possible for the extreme Si/Mg values. Within the shaded region is the mass-radius curve (pink dashed line) for the mean Si/Mg value found in Hypatia

```
pip install exoplex
```

Required Python libraries, listed in table 3.3, are automatically installed with pip. The additional requirement of the Perple_X software package is installed by ExoPlex

upon the first instance of its use.

Table 3.3

Third party libraries required for running ExoPlex.

Library	Version	Use
numpy	1.14.4	array handling
matplotlib	2.2.2	plotting
pexpect	4.4.0	opens a terminal to query Perple_X
multiprocessing	2.6.2.1	Perple_X for upper and lower mantle in parallel
burnman	0.9.0	core equation of state
Additional libraries		
Perple_X*	6.8.1	mantle mineralogy solver and equation of state

*Automatically downloaded and added to the exoplex library if Perple_X is needed

3.4.1 Development environment

Users must setup the appropriate environment to successful run scripts containing ExoPlex routines. This is due to the dependence upon phase equilibria solution files. These files require a substantial computational load to create so it is best that the user keeps generated files in a folder for later use rather than recreating these files each time ExoPlex is used. Below is an example of the directory tree where users should develop their scripts.

```
Exoplex folder                                                    myscript.
```

Where myscript.py is where the ExoPlex functions should be called from. All Perple_X results will be stored in the Solutions/ folder automatically. The options for running Perple_X are stored in the Options/ folder. The options file is used by Perple_x

to select solution equilibrium parameters and output options. More specific details of each parameter can be found on the Perple_X website. The solutions_model.dat file contains the mineral phase thermodynamic data modified from Stixrude & Lithgow-Bertelloni (2011). These two files must be downloaded from the ExoPlex GitHub page. Users may simply download the development environment from the same page which includes a compressed file with precompiled phase equilibria solutions and the .dat files above.

3.4.2 Selected functions

While the functionality is described in a separate readMe document, it is worthwhile to mention several important features of the code. For every graphical output in ExoPlex, the user is able to send the results to a file for their own analysis. When creating a planet model, there are multiple modes by which a user may define their planet. The user must first decide whether to fix the mass or radius. ExoPlex only creates models of radius as a function of mass. In order to solve for mass with an input radius, we invert the same model using a bisection technique where we adjust the mass to fit the radius. Doing so adds extra computation time so the models of radius as a function of mass are quicker.

The model composition must also be specified. Users have the ability to take two routes: enter the bulk composition of the planet along with the core composition, or enter the core mass fraction and the composition of the core and mantle separately. In the former case, ExoPlex will convolve the bulk and core inputs to solve for the core mass fraction and the mantle composition. The latter case allows for users to directly set the mantle composition and core mass fraction. In this section we review two of the modeling options currently available in ExoPlex.

Mass-radius diagram

The relationship between mass and radius of incompressible bodies can give clues to a planet's bulk composition and internal structure Zapolsky & Salpeter (1969). In the context of exoplanets, mass-radius diagrams have become valuable tools for first-order approximation of planet type (Seager et al., 2007; Valencia et al., 2006; Sotin et al., 2007). Generally, this is achieved by plotting the mass and radius of planets with various internal mass distributions. All planets with measured mass and radius should fit somewhere between 100% iron, the densest planet expected, and 100% gas or water, the least dense case. ExoPlex is not equipped with a gas phase model so we use liquid/ice H2O for our low density limit. Each planet is then characterized to first order by their core, mantle and water mass fractions (CMF+MMF+WMF = 1.0).

The proportions of these three layers largely determine the bulk density of planets. Mantle composition has only a secondary influence. The advantage of using ExoPlex is that users may plot planets based off of their bulk elemental abundances of Fe, Mg, and Si. This provides an immediate link to the host star composition in addition to an insight of the possible internal structures (CMF, MMF, WMF). Planets are not expected to perfectly mirror their host stars in composition; however, they do initially form from the same material in the solar nebula. Departures from initial composition may offer clues to how the planet evolved over time through cometary water delivery or post-formation impacts as seen in figures 3.4 and 3.5.

Radial profiles

ExoPlex also has a function to produce a single (or a few) planets of a specific mass and composition for a more detailed analysis. The built-in plotters use the matplotlib

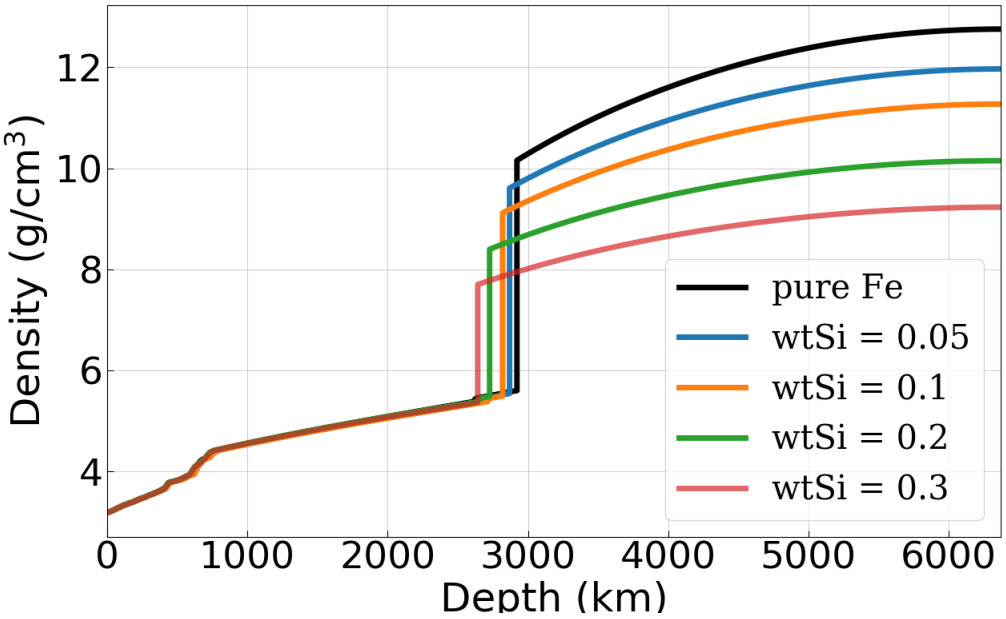

Figure 3.8

Radial density plots of planets with mass or 1 $M_{\oplus}$, and core mass fraction fixed at CMF = 32.3%. Core composition is varied by adding Si by wt%. The black curve is a model with a pure iron core while the other curves have between 5 and 30% Si cores by mass. For an increasing fraction of Si alloy, the core becomes less dense and therefore larger.

libraries with a predetermined theme to produce figures of radial profiles of density, mass, mineralogy, pressure, temperature, and thermodynamic parameters. These functions also allow users to store the data in separate text files for later use.

Figure 3.8 shows an ExoPlex-generated example of the radial density profile for several models. In this example, we vary the core composition from pure liquid iron to an alloy of 70$ and 30% Si. These curves demonstrate the significance of core composition. While it would be difficult to constrain the exact composition of an exoplanet core, we can impose limits upon the possible compositions by convolving

available data on mass, radius, and bulk planet composition (from the host star). Indeed, this detail may not be necessary for current observational accuracy but, leaving the option to have a more realistic model of exoplanet cores that contain components other than iron (as is the case for Earth), may influence the desire for more accurate observations and promote exploratory modeling until such data are available.

3.5 Model sensitivity analysis

3.5.1 Model variation within a range of parameters

In this section, we perform an investigation into the sensitivity of model results to the various inputs. Currently the focus of astronomers is to collect mass and radius data on exoplanets. It has been demonstrated above and other works that mass and radius data can be used to uniquely constrain the core and mantle mass distributions within dense planets; for lighter planets, a low-density component must be included. This is possible only if some core and mantle composition is assumed. It has been suggested that mass and radius are essentially invariant within the known regime of rocky planet compositions (Seager et al., 2007; Valencia et al., 2006; Zeng & Sasselov, 2013). Recent work by Dorn et al. (2015) however, has indicated the usability of host star composition as an indicator or planet composition. Here we analyze the viability of using host star abundance measurements in constraining planetary composition.

In Table 3.4 we report the results of radius as a function of mass and composition models. All parameters are initially set to the canonical Earth vales (Table 3.2) and then each is allowed to vary along a reasonable range while the other parameters remain fixed. The four parameters shown are: Fe/Mg_{bulk}, Si/Mg_{bulk}, $wtSi_{core}$, and XFeO. Table 3.4 has these parameters ranked by influence upon the model. The first two can possibly be inferred from the host star, while the latter two cannot. While

the possibly measurable parameters exert a respectable influence on the model, these are currently within expected observational uncertainties. In spite of this, the most interesting parameter, Fe/Mg_{bulk} exerts a nearly detectable influence. Knowing this value would be highly valuable because it enables one to restrict the possible core sizes considerably.

3.5.2 Parameter correlation with results

Of the parameters listed in Table 2.1, not all are measurable. Only mass and radius are reliably inferred from observations. It has been shown that host star composition can be used as an indicator of most likely solutions to measured mass and radius (Dorn et al., 2015), so we include $(Fe/Mg)_{bulk}$, $(Si/Mg)_{bulk}$ as worthwhile measurables; assuming similarity between host star and planet composition. While no other parameter for our model can be detected, it is prudent to test the influence of all model components. To this end, we created a discrete grid of models with a range of input parameters. We chose to fix the mass at $M = 1$, 2.5 or 5 $M_\oplus$ while varying all other parameters. The ranges are listed in Table 3.5 along with the correlation parameters for two correlation metrics discussed below. The radii min/max values represent the global min/max for each range of input parameters. Note that this does not necessarily mean that these values are a result of the max/min of the input parameters.

Our sensitivity test is to calculate the Pearson correlation coefficient for each variable. It is a measure of the linear correlation between two variables made by normalizing the covariance of the two variables with the product of their standard deviations. For variables X, Y, their general comoving trend can be deciphered by calculating their covariance. The covariance of two variables, one which may be

Table 3.4

Individual parameters are varied while others are fixed at nominal Earth values (table 3.2). The total range in radii are reported across a reasonable range in model parameters. The same analysis is performed for 1,2.5, and 5 $M_\oplus$ planet models.

		Total % variation in radius		
Parameter	**range**	**1 $M_\oplus$**	**2.5 $M_\oplus$**	**5 $M_\oplus$**
Fe/Mg_{bulk}	[0.35,1.32]	6.1%	6.4%	6.5%
$^*Si/Mg_{bulk}$	[0.56,1.95]	2.4%	2.8%	3.1%
$wtSi_{core}$	[0,20%]	0.17%	0.18%	0.18%
XFeO	[0,0.2]	0.25%	0.19%	0.11%

* $Si/Mg_{bulk} = Si/Mg_{mantle}$

Table 3.5

List of model parameters and their correlation with resulting radius. Mass fixed at 1 $M_\oplus$. Pearson and Spearman correlation coefficients all significant to the 0.05 level.

Parameter	range	Pearson	Spearman
WMF	[0,1]	0.9368	0.9525
Fe/Mg_{bulk}	[0.05,53.5]	-0.5210	-0.5907
$^*Si/Mg_{bulk}$	[0.15,2.05]	0.0159	0.0158
Fe/Mg_{mantle}	[0.05,2.05]	-0.0566	-0.0580
CMF	[0,1]	-0.7378	-0.6969
MMF	[0,1]	-0.1990	-0.2102

* $Si/Mg_{bulk} = Si/Mg_{mantle}$

dependent of the other, is

$$\mathrm{cov}(X, Y) = E[(X - E[X])(Y - E[Y])], \tag{3.1}$$

where $E[X]$, the expected value, is the mean of X. Positive values for the covariance indicates a mutually increasing trend whereas a negative value shows the variables are inversely related; in other words as X increases Y decreases. $\mathrm{cov}(X, Y)$ is only a reliable measure of relatedness between the two variables. To understand the relative magnitude of the covariance, we must normalize it. We use the product of the standard deviations of X and Y to find the Pearson correlation coefficient,

$$\rho_{XY} = \frac{\mathrm{cov}(X, Y)}{\sigma_X \sigma_Y}. \tag{3.2}$$

The values of ρ_{XY} fall in the range [-1,1], where a 1 indicates a perfectly positive linear relationship, -1 is a linear relationship with a negative slope, and values near 0 suggest that there is no correlation between X and Y. Generally, absolute value of the correlation coefficients, $|\rho_{XY}|$, more than zero are an indicator of some relationship, however, the significance of the correlation depends on context. In this study, we will only compare the relative magnitudes of ρ_{XY} in order to rank the input parameters.

For data that are nonlinear, it might be better so assess the relationship of two variables in terms of their mutual directions of change independent of their rate of change. Similar to the Pearson correlation coefficient, Spearman rank correlation coefficients meausre the relatedness of two variables in terms of their general trend. Spearman rank coefficients test the monotony of two variables, i.e., whether or not they mutually trend. This allows for an estimate of relatedness of any type. At the two extremes, -1 and +1, the variables have a perfectly linear relationship.

Applying this to the effects of varying the input parameters listed in Table 3.4, it is seen that radius correlates very strongly with water mass fraction, WMF. Next in importance are the core mass fraction, CMF, and the similar quantity, the bulk Fe/Mg ratio. The bulk Si/Mg abundances, and the Fe/Mg ratio in the mantle, have the weakest effect on the planet radius.

Chapter 4

DISCUSSION

4.1 Assumptions made

In creating any model of a physical phenomenon, there are accompanying assumptions made. The ExoPlex code is no exception. Below we review the assumptions made to model rocky exoplanets.

1) ExoPlex models planets with bulk composition similar to the terrestrial planets in the solar system. It has been proposed that this is not the only characteristic terrestrial planet type. Planets that form in a nebula depleted in oxygen may be carbonaceous in composition (Kuchner & Seager , 2005). A carbon planet can be differentiated in the same way rocky planets are except with a mantle composed mostly of SiC or graphite, in addition to a core of mostly Fe. For C/O ratios at least twice that of the solar C/O ratio of C/O=0.5, carbon can become dominant in the planet formation process by using up the oxygen budget to form CO.

The excess carbon can plausibly form low-mass planets. The formation pathway of carbon planets has been studied, but to date, there has been less interest in modeling this type of planet as a possible class of solid exoplanets. Seager et al. (2007) modeled carbon planets with a solid iron core and either graphite or SiC mantles. They found little difference in the mass-radius relationship of these carbon planets compared to the silicate dominant planets. With this in mind, it would be impossible to infer whether a planet is carbon or silicate dominant without a reliable measure of the host star's C/O ratio. To date no carbon planet is known. A search of the Hypatia catalog (Hinkel et al., 2014) shows that C/O ratios above solar, while not abnormal, are never

seldom go above C/O = 1, indicating that carbon-rich systems might exist but would be rare. For these reasons we chose not to develop a model for carbon planets. As the number of planet hosting stars with measured photospheric abundances grows, it may become prudent to reconsider carbon planets.

2) To make reasonable models of mantle mineralogy, ExoPlex must assume a temperature profile. We usually impose a temperature gradient, increasing monotonically with depth, corresponding to an adiabatic geotherm, assuming that mixing within the mantle leads to an isentropic temperature profile. This is a necessarily best guess, considering that we do not know what the true temperature gradient is for rocky exoplanets. The temperature gradient in the Earth's mantle is not known with perfect certainty, but tends to rise about 0.5 K per kilometer of depth, which is steeper than the adiabatic gradient. This implies imperfect heat transport by convection, plus thermal inputs from radioisotopes. We do not include thermal contributions from radioactive components, nor heating from the core, and do not model the transport of heat through the mantle. Heat transfer within the earth takes several modes depending on location and depth. The inner core is conductive while the outer core is convective. The enhanced heat transfer from the outer core serves to efficiently heat the lower mantle thus being a significant component to mantle convection. Radiogenic heating reduces the viscosity in the mantle which also contributes to convection. We cannot reasonably assume all of these processes occur on other planets, and to model them would introduce excessive layers of uncertainty to our model.

Our default assumption is that the temperature gradient is adiabatic, but ExoPlex does allow for users to input various central and surface temperatures. In many cases, estimates of a planet's surface temperature can be determined by using the host star's luminosity with the planet's inferred semi-major axis to at least calculate the effective surface temperature. Including details of atmospheric extent and composition could

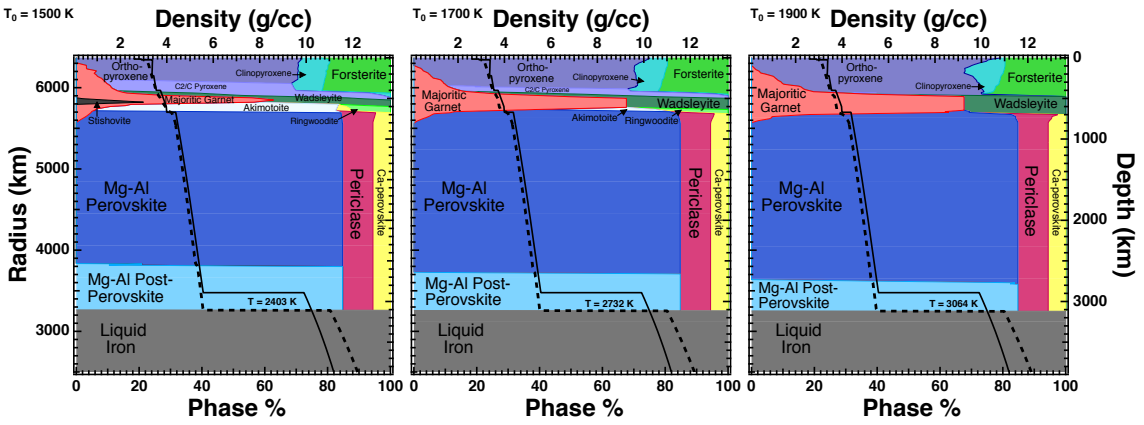

Figure 4.1

Mineral phase diagrams generated by ExoPlex. Percentage of mass contribution of each mineral phase at depth is shown on the horizontal axes. Each diagram is a model of a $1R_{\oplus}$ radius planet with bulk composition equivalent to solar values from Lodders (2003). The surface temperatures are varied from T_0 = 1500, 1700 and 1900 K (left to right). The solid lines are Earth's geotherm whereas the dotted lines represent the model geotherms assuming an adiabat. The surface temperatures provide a starting point for the geotherm which in result, shifts the location in the phase diagram, for these planets. Upper-mantle mineralogy is highly sensitive to this starting point. For the higher pressures seen in the lower mantle, in contrast, the resultant mineralogies are identical.

make the estimate of the surface temperature T_0 more robust. Variations in the surface temperature do not significantly change the mass-radius relationship, but they do have an effect on the upper mantle mineralogy, as illustrated in Figure 4.1).

While variations in temperature profile and upper-mantle mineralogy would not impart a measurable impact in the mass-radius relationship of a planet, models with a water layer see large variations in radius with variations in surface temperature. For a reasonable value of surface pressure on planets without overwhelming atmospheres,

as is the case of Neptunian-type planets, ExoPlex allows for surface H_2O to be liquid or ice Ih (see our assumed phase diagram in Figure 2.4).

3) The ExoPlex modeling assumes the measured radius of the planet is not significantly altered by an atmosphere. Low-mass planets are not generally considered to have atmospheres with sufficiently large scale height and density to influence radius measurements, but planets larger than 1.6 Earth radii do (Weiss & Marcy 2014; Rogers 2014; Chen & Kipping 2017). Because ExoPlex does not include a treatment for gas envelopes, this limits the viability of the model to results for planets less than $\sim 1.6 R_\oplus$ in radius, or about $4 M_\oplus$ in mass.

Multiple works show that this is the mass and radius above which exoplanets have atmospheres, for which ExoPlex would be inapplicable. Weiss & Marcy (2014) analyzed mass and radii of exoplanets less than $4\,M_\oplus$. They found that below a radius of $1.5\,R_\oplus$, planets tend to be denser than planets above that radius. It is likely that exoplanets larger than this general radius have atmospheres sufficiently thick to influence the radius observations. Planets near the upper limit considered, $\approx 4 M_\oplus$, have densities $\sim 1\,\mathrm{g\,cm^{-3}}$. Even including thick water envelopes, it is necessary to include H_2/He atmospheres. Chen&Kipping (2017) showed that there exists a fundamental empirical mass-radius relationship for all exoplanets. For planets less than about $2\,M_\oplus$, planet radius grows roughly as $R \propto M^{0.28}$, close to the incompressible limit $R \propto M^{1/3}$, but allowing for some compressibility of rock. They dubbed these planets "Terran planets". For planets larger than about $2 M_\oplus$, they found a different mass-radius relationship, $R \propto M^{0.59}$, albeit with more scatter around this trend. This indicates that planet densities are lower at higher masses, strongly suggesting low-density atmospheres. The neglect of atmospheres by ExoPlex is almost certainly unjustified for planets greater than about $4\,M_\oplus$, and perhaps as small as $2\,M_\oplus$. There are caveats to this limit, though. Empricial mass-radius relationships are based on

averages of planets, but individual rocky exoplanets may devaite from these trends. Retention of atmospheres is also a strong function of insolation and proximity to the host star,

4) ExoPlex must extrapolate equation of state data for exoplanets that deviate from Earth-like: very massive rocky planets that will experience extreme pressures in their lower mantles, and for planets with distinctly non-terrestrial compositions. The data used for the mantle and core were developed with the Earth in mind. This creates a bias in accuracy towards planets with characteristics similar to Earth. Applying the same equations to planets that diverge from Earth's mass and composition implies an uncertain extrapolation beyond intrinsic conditions.

Extrapolations introduce uncertainties in three ways. First, an exoplanet may be massive enough to generate lower-mantle pressures that could lead to denser polymorphs than are included in the database. Based on the likely presence of dense atmospheres, we already recommend that ExoPlex not be used to model planets above a few Earth masses, and this same caveat applies to the uncertainty in lower-mantle mineralogy. Second, depending on what geotherm is assumed, the range of model temperatures may exceed the range in mineral databases, even at moderate pressures. Third, by allowing users to choose arbitrary mantle compositions, very likely, some low-pressure minerals may exist for which adequate thermodynamic data do not exist.

Earth's mantle spans a range in pressure of up to 136 GPa. The most complex diversity of minerals occurs only in the upper mantle; the lower mantle is relatively simple. Phase transitions occur more rapidly along a shallow pressure gradient than they do at the high pressures of the lower mantle, as is seen in Earth's density profile (Dziewonski & Anderson, 1981) (Figure 2.3), in which the rapid variation of mineralogy and density with depths is caused by multiple phase transformations

into denser polymorphs; in contrast, the lower mantle below 660 km has smooth variations in density, indicating single polymorphs of ringwoodite, or periclase and perovskite. On other Earth-mass planets with non-Earth-like Mg/Si and other ratios, one may expect some combination of magnesiowstite ((Mg,Fe)O), stishovite (SiO_2) and perovskite ((Mg,Fe)SiO_3 or $CaSiO_3$) below this depth for an Earth mass planet. We take advantage of this, we split the mantle of an exoplanet into an upper and lower mantle, with the threshold at 125 GPa. At greater depths than this level, we assume with some confidence that the mineralogy is simply magnesiowüstite, bridgmanite, and (at even greater pressures), post-perovskite. This means that we can use a coarser grid of Perple_X generated mineral properties at high pressures, speeding up computation times; but it also means that we purposely neglect some possible polymorphs at high pressures.

5) ExoPlex lacks equation of state data for the core. The core overall is much simpler, mineralogically, than the mantle. In spite of this, the core is not as well understood on Earth as is the mantle. Our model for the core builds only on what is known of Earth's core. Earth's core is predominantly Fe/Ni. (Ni is similar in mass and chemical properties to Fe, and essentially can be replaced in models by Fe). But the core is not entirely Fe/Ni: it is well-known that there exist density deficits which point to the presence of some mass fraction of light alloying elements (Poirier, 1994; Anderson & Ahrens, 1994; McDonough, 2003; Valencia et al., 2006). Since Earth's core has a roughly 10 wt% density deficit, these light alloys should not be neglected when we look at planets in other systems. While the core composition of exoplanets may never be detectable, the density deficit caused by non-pure Fe/Ni cores can impact core size and state, and in turn geophysical processes. Leaving the possibility of non-singular core composition elevates degeneracy in the solution, but it allows us to remain open minded to the plethora of possibilities. Our consideration

of non-singular composition cores is unique among similar models.

The light element (not Fe or Ni) content of Earth's core is still debated and arguments for S, Si, O or some combination of the three are all plausible (Poirier, 1994). While many components have been suggested for Earth's core, Si, S, and O likely dominate in both presence and impact on the core size. The mineralogical system we use for the core is much simpler than the system we use for the mantle: just Fe, FeS, FeSi and FeO. Despite this, the equations of state and polymorphs for these components at core conditions are poorly understood. Because data are lacking, we do not try to model the exact mineralogy. Instead, we take the best defined and prevalent material, pure Fe, and allow the alloys to manifest themselves simply through a reduction of the reference density used in the equation of state, ρ_0. For Earth's core, light elements effectively lower the molar mass of the core but have almost no effect on the compressibility of the core Anderson & Ahrens (1994). We extend this finding to arbitrary abundance of the included light elements; however there are limitations to this practice. Anderson & Ahrens (1994) reported that the second derivative of the bulk modulus does deviate with slight compositional differences due to the introduction of light elements to Fe. To first order, the compressibility of pure Fe remains only slightly perturbed for a 10% (Earth-like) density deficity attributable to light elements. For models with more light element content, the bulk modulus and its derivatives are expected to vary substantially, compromising the validity of results. As such we suggest users use this feature with caution and keep light element inclusions to a reasonable amount similar to what is expected of the earth.

Chapter 5

CONCLUSION

Future work

Future work on the ExoPlex code should include a more detailed temperature model that connects the mantle with the core and surface. The temperatures at both boundaries are uncertain, however. Estimates of stellar insolation can be made by first considering the equilibrium temperature of planets. Estimates of of both stellar spectral type and planet semi-major axis for confirmed exoplanets have already been made for planets detected by both the radial velocity and transit methods. With these, the blackbody temperature of a planet with no atmosphere and assumed albedo can be found. Of course, even relatively small atmospheres like the Earth's can raise the surface temperature substantially via the greenhouse effect. Thus exoplanet models should include a full atmospheric model to constrain the surface temperature properly. This would, unfortunately, require knowledge of the volatile abundances, in addition to stellar insolation. Even a crude model of H-C-N-O bearing molecules would be an improvement, allowing a model of a terrestrial planet with all the layers such an exoplanet is thought to have: core, mantle, H_2O layer, and atmosphere. The effect of surface temperature is not as important as the internal temperature, though.

Better modeling of the internal temperature could yield significantly more accurate exoplanet models. For instance, the ExoPlex code does not currently have the ability to differentiate between solid and liquid core states. The ramifications of a solid core could be decreased loss of a planet's primordial heat budget and the lack of a magnetic field. The mantle geotherm can be modeled for the range of compositions,

but the thermodynamic properties of materials at core conditions are less certain. The core composition would need to be known to generate conclusions on its state. This introduces a new set of uncertainties that cannot be inferred from mass and radius. Valencia et al. (2006) found that they can produce fully solid or partially liquid cores for every planet mass in their model by varying the Grneisen parameter in their geotherm within reasonable values. Reproduction of accurate cores could be accomplished by better thermodynamic data and better modeling of the core temperatures.

As ExoPlex is increased in complexity, the number of parameters expands beyond the number that can be constrained by the limited amount of available exoplanet data. Observable bulk properties of exoplanets like the radius (for a given mass) are insensitive to variations in internal state and composition, and so the large number of parameters become highly degenerate for plausible model solutions. Such modeling is worthwhile anyway, because a more detailed model can provide an interesting exploration into the planet populations to look for by modeling synthetic planets. One strategy for coping with the degeneracies is to consider parameters probabilistically rather than deterministically. Not all inputs will be equally probable for all degenerate solutions. In situations like this where data are limited for a model with many parameters, a Bayesian-based model inversion can determine both model sensitivity and the probability of certain inputs. Bayesian statistics can take advantage of any data that is available by using conditional probability in a holistic manner. Each parameter is examined for its influence on the desired results which are in this case, the data (mass radius, bulk composition from the host star, etc.). More influential parameters like bulk Fe/Si will have a higher degree of certainty than other. Even less significant parameters would be made less ambiguous in this technique. Such a model can be easily expanded to include new data parameters as technology and methods

improve. ExoPlex is not yet optimized to perform this task. A Markov-Chain Monte Carlo inversion would require at least ∼10,000 calls to ExoPlex. This is not ideal considering each new model takes roughly two minutes to complete for the lowest mantle resolution, but is a future goal.

Conclusion

This thesis has presented a comprehensive model for rocky exoplanets below about 4 $M_{\oplus}$. Because of the relatively low availability of such tools, we have adapted our code into a Python library and made the source code available on GitHub. Users of ExoPlex can now create rocky planets using their own scripts, giving them full flexibility to manage results. Written in a modular fashion, the code can be expanded to include more functionality and create an overall more robust model. In the meantime, ExoPlex is at a level of detail which is properly in line for modern observations of exoplanets. That is, the code does not require excessive assumptions to be connected to observed planets. With only mass, radius, and possibly inferred bulk composition from host stars, users can create a realistic internal model of confirmed exoplanets.

REFERENCES

Bernardi G. et al., 2016, arXiv:1606.06006

Anderson, W. W., Ahrens, T.J. (1994) Journal of Geophysical Research. vol. 99 4273-4284.

Batalha N. M., Borucki W. J., Bryson S. T. et al. (2011) ApJ 729 27.

Belonoshko, A. B. (2010). Condens. Matter. Phys., 13, 23605

Bezacier, L., Journaux, B., Perrillat, J.-P., Cardon, H., Hanfland, M., Daniel, I.(2014). The Journal of Chemical Physics 141, 104505. https://doi.org/10.1063/1.4894421

Birch, F. (1947). Physical Review. 71 (11): 809824. Bibcode:1947PhRv...71..809B. doi:10.1103/PhysRev.71.809

Birch, F. (1964) Journal of Geophysical Research. Vol. 69. No. 20

Cassan, A., Kubas, D.,..., Wyrzykowski, L. (2012) Nature. Vol.481 pg. 167 doi:10.1038/nature10684.

Charbonneau, D., Brown, T.M., Latham, D.W. and Mayor, M., 1999. The Astrophysical Journal Letters, 529(1), p.L45.

Chen, J., Kipping, D. (2017). The Astrophysical Journal, 834:17 (13pp). doi:10.3847/1538-4357/834/1/17.

Connolly, J. (2009) Geochemistry, Geophysics, Geosystems, 10, Q10014.

Cottaar, S., Heister, T., Rose, I., Unterborn, C. (2014). Geosystems, 15 (4) , 1164-1179, doi: 10.1002/2013GC005122, url: http://doi.wiley.com/10.1002/2013GC005122

Dziewonski, A. M., and D. L. Anderson. (1981). Phys. Earth Plan. Int. 25:297-356. doi:10.17611/DP/9991844

Pepe, Francesco A.; Cristiani, Stefano; Rebolo Lopez, Rafael; Santos, Nuno C. ..., Zerbi, Filippo. doi: 10.1117/12.857122

Foley, B. ApJ, 812:36 23pp, (2015) October 10 doi:10.1088/0004-637X/812/1/36

Donati, J.F., Delfosse, X. , Artigau, E., Doyon, R. (2014) SPIROU-2000-IRAP-RP-00503.

Dorn, C, Khan, A, Heng, K, Alibert, Y, Connolly, J, Benz, W, & Tackley, P (2015) Astronomy & Astrophysics 577 A83.

Dorn, C., Venturini, J., Khan, A., Heng, K., Alibert, Y., Helled, R.(2017) Astronomy & Astrophysics 597, A37. DOI: 10.1051/0004-6361/201628708.

Dorn, C, Khan, Hinkel, N., Venturini, J. (2017b) Astronomy & Astrophysics 597, A38. DOI: 10.1051/0004-6361/201628749.

Fei Y., Mao H. K., and Hemley R. J. (1993) J. Chem. Phys. 99, 53695373.

Gillon, M. A. et al. (2016) Nature 533, 221224.

Gillon, M. et al. (2017) Nature 542, 456460.

Helffrich, G.R., Wood, B.J. (2001) Nature. volume 412, pages 501507.

Hinkel, N. R., Timmes, F.X., Young, P.A., Pagano, M. D., Turnbull, M.C. (2014). The Astronomical Journal, Volume 148, Issue 3, article id. 54, 33 pp.

Ito, E. & Takahashi, E. J. Geophys. Res. 94, 1063710646 (1989).

Kuchner, M. & Seager, S., Extrasolar Carbon Planets, arXiv:astro-ph/0504214.

Labrosse, S., Poirier, J.P., Mouel, J.-L., (2001) Earth and Planetary Science Letters, 190, p. 111-123.

Léger, A., Selsis,F., Sotin, C., Guillot, T., Despois, D., Mawet, D., Ollivier, M. (2004). Icarus. 169 499504.

Liu, L. Nature 262, 770772 (1976).

Lodders, K. 2003, ApJ, 591, 1220

Lopez, E., Fortney, J. (2014) The Astrophysical Journal, Volume 792, Number 1.

Lovis, C., Fischer, D.(2011). University of Arizona Press, 526 pp. ISBN 978-0-8165-2945-2., p.27-53

Mayor, M. & Queloz, D., Nature 378, 355359 (23 November 1995)doi:10.1038/378355a0

Mayor, M. et al. 2003, The Messenger 114, 20.

Mayor, M., Bonfils, X., Forveille, T., Delfosse, X., Udry, S., Bertaux, J.-L., Beust, H., Bouchy, F., Lovis, C., Pepe, F., Perrier, C., Queloz, D., and Santos, N.C. (2009). A&A 507, 487494. DOI: 10.1051/0004-6361/200912172

McDonough, W.F., 2003

Poirier, J.P. (1994) PEPI. 85, 319.

Rivera, E. et al. (2005) The Astrophysical Journal. Volume 634, Issue 1, pp. 625-640.

Rogers, L. , Seager, S. 2010

Seager, S, Kuchner, M, Hier-Majumder, C, & Militzer, B (2007) Astrophysical Journal, 669, 1279

Sarkis, P., Henning, T., Krster, M., Trifonov, T., Zechmeister, M., ...Montes, D. (2018)., ApJ, 155, 6.

Sotin, C., Grasset, O. Mocquet, A. (2007). Icarus 191, 337-351.

Stixrude, L. & Lithgow-Bertelloni, C. (2005) Geophysical Journal, Volume 162, Issue 2, pp. 610-632.

Stixrude, L. & Lithgow-Bertelloni, C. (2011) Geophysical Journal International, 184, 3.

Tian. F & Ida, S. (2015) Nature Geoscience volume 8, pages 177180

Umemoto, K., Wentzcovitch, R. M., Wu, S., Ji, M. Wang, C., Kai-Ming Ho. (2017), Volume 478, 2017, Pages 40-45, ISSN 0012-821X, https://doi.org/10.1016/j.epsl.2017.08.032.

Unterborn, C., Dismukes, E.E., Panero, W.R. (2016). ApJ 819, 32.

Unterborn, C. Hinkel, N. 2017 in prep.

Unterborn, C.T., Desch, S.J., Hinkel, N.R., Lorenzo, A. (2018) Nature Astronomy. volume 2, pages297302.

Valencia, D., OConnell, RJ, & Sasselov, D (2006) Icarus, 181, 545.

Valencia, D., Sasselov, D., OConnell, R.J. (2007) The Astrophysical Journal, Volume 656, Issue 1, pp. 545-551.

Valencia, D., Sasselov, D., OConnell, R.J. (2007) The Astrophysical Journal, Volume 665, Issue 2, pp. 1413-1420.

Vinet, P., Smith, J.R., Ferrante J., and Rose, J.H. (1987). Physical Review B. 35: 19451953. doi:10.1103/physrevb.35.1945.

Weiss, L.M., Marcy, G.W. (2014). The Astrophysical Journal Letters, 783:L6.

Wolszczan, A., Frail, D. A. (1992). Nature. 355 (6356): 145147. Bibcode:1992Natur.355..145W. doi:10.1038/355145a0

Wolszczan, A. (1994). Science. 264 (5158): 538542. doi:10.1126/science.264.5158.538.

Wright, J.T., Gaudi, S. (2012) arXiv:1210.2471

Yoder C. F. (1995). Astrometric and geodetic properties of the Earth and the solar system. In Global Earth Physics: A Handbook of Physical Constants. Vol. AGU Reference Shelf (ed. T. J. Ahrens). American Geophysical Union, Washington, DC, pp. 131.

Zapolsky, H. S., Salpeter, E. E. (1969). Astrophysical Journal, vol. 158, p.809. DOI:10.1086/150240

Zeng, L., Sasselov, D. (2013). Astronomical Society of the Pacific, Volume 125, Issue 925, pp. 227. DOI:10.1086/669163.

Zeng, L. Dimitar D. Sasselov, and Stein B. Jacobsen. (2016) ApJ, 819, 127.

APPENDIX A

CALCULATING STRUCTURE FROM STOICHIOMETRY

The mass distributions of material int he core and mantle are found using stoichiometry. Both the core and mantle have fixed chemical components which are combined to form minerals present at depth given pressure, temperature, and the Gibbs free energy minimization scheme of perple_X. The mantle includes the following oxides: SiO_2, FeO, MgO, CaO, and Al_2O_3. For the core: Fe, FeO, FeS, and FeSi. Together with the input parameters, stoichiometry and hence core mass fraction is well-defined.

The bulk abundance ratios are in terms of mole ratio. Below, we show how the compositional inputs outlined in table 2.1 are defined such that they relate to a molar abundance of each element through the use of a fixed number of chemical components in the model. For reference, the $N_{X_(c,m}$ variables represent the number of moles of element, X present in the core (c) or mantle (m) and m_X is the mass of element X in atomic mass units. So N_{Si_c} refers to the number of Si moles in the core.

$$N_{O_m} = 2N_{Si_m} + N_{Fe_m} + N_{Mg_m} + N_{Ca_m} + \frac{3}{2}N_{Al_m} \tag{A.1}$$

$$N_{Fe_c} + N_{Fe_m} = \left(\frac{Fe}{Si}\right)_{bulk} (N_{Si_c} + N_{Si_m}) \tag{A.2}$$

$$N_{Mg_m} = \left(\frac{Mg}{Si}\right)_{bulk} (N_{Si_c} + N_{Si_m}) \tag{A.3}$$

$$N_{Ca_m} = \left(\frac{Ca}{Si}\right)_{bulk} (N_{Si_c} + N_{Si_m}) \tag{A.4}$$

$$N_{Al_m} = \left(\frac{Al}{Si}\right)_{bulk} (N_{Si_c} + N_{Si_m}) \tag{A.5}$$

$$X_{FeO} = \frac{N_{Fe_m}}{N_{Fe_m} + N_{Fe_c}} \tag{A.6}$$

$$Si_c wt = \frac{N_{Si_c} m_{Si}}{N_{Fe_c} m_{Fe} + N_{Si_c} m_{Si} + N_{O_c} m_O + N_{S_c} m_S} \tag{A.7}$$

$$O_c wt = \frac{N_{O_c} m_O}{N_{Fe_c} m_{Fe} + N_{Si_c} m_{Si} + N_{O_c} m_O + N_{S_c} m_S} \tag{A.8}$$

$$S_c wt = \frac{N_{S_c} m_S}{N_{Fe_c} m_{Fe} + N_{Si_c} m_{Si} + N_{O_c} m_O + N_{S_c} m_S} \tag{A.9}$$

$$\begin{aligned} M_P = N_{Fe_c} m_{Fe} + N_{Si_c} m_{Si} + N_{O_c} m_O + N_{S_c} m_S + N_{Fe_m} m_{Fe} + ... \\ N_{Mg_m} m_{Mg} + N_{Si_m} m_{Si} + N_{O_m} m_O + N_{Ca_m} m_{Ca} + N_{Al_m} m_{Al} \end{aligned} \tag{A.10}$$

The goal is to solve for the mole values of each element in the core and mantle. To do this every term that is a multiple of an independent variable (i.e. N_xs is combined and moved over to one side of the equation. These equations appear below.

$$-N_{Fe_m} - 2N_{Si_m} - N_{Mg_m} + N_{O_m} - N_{Ca_m} - \frac{3}{2}N_{Al_m} = 0 \tag{A.11}$$

$$N_{Fe_c} - \left(\frac{Fe}{Si}\right)_{bulk} N_{Si_c} + N_{Fe_m} - \left(\frac{Fe}{Si}\right)_{bulk} N_{Si_m} = 0 \tag{A.12}$$

$$-\left(\frac{Mg}{Si}\right)_{bulk} N_{Si_c} + N_{Mg_m} - \left(\frac{Mg}{Si}\right)_{bulk} N_{Si_m} = 0 \tag{A.13}$$

$$-\left(\frac{Ca}{Si}\right)_{bulk} N_{Si_c} - \left(\frac{Ca}{Si}\right)_{bulk} N_{Si_m} + N_{Ca_m} = 0 \tag{A.14}$$

$$-\left(\frac{Al}{Si}\right)_{bulk} N_{Si_c} - \left(\frac{Al}{Si}\right)_{bulk} N_{Si_m} + N_{Al_m} = 0 \tag{A.15}$$

$$X_{FeO}N_{Fe_c} + (X_{FeO} - 1)N_{Fe_m} = 0 \tag{A.16}$$

$$Si_c wt(N_{Fe_c}m_{Fe} + N_{O_c}m_O + N_{S_c}m_S) + (Si_c wt - 1)N_{Si_c}m_{Si} = 0 \tag{A.17}$$

$$O_c wt(N_{Fe_c}m_{Fe} + N_{Si_c}m_{Si} + N_{S_c}m_S) + (O_c wt - 1)N_{O_c}m_O = 0 \tag{A.18}$$

$$S_c wt(N_{Fe_c}m_{Fe} + N_{O_c}m_O + N_{Si_c}m_{Si}) + (S_c wt - 1)N_{S_c}m_S = 0 \tag{A.19}$$

$$\begin{aligned} M_P = {} & N_{Fe_c}m_{Fe} + N_{Si_c}m_{Si} + N_{O_c}m_O + N_{S_c}m_S + N_{Fe_m}m_{Fe} + ... \\ & N_{Mg_m}m_{Mg} + N_{Si_m}m_{Si} + N_{O_m}m_O + N_{Ca_m}m_{Ca} + N_{Al_m}m_{Al} \end{aligned} \tag{A.20}$$

There are **10 unknowns** (Mole numbers) and thus **10 equations** relating them. Four components to the core and six components to the mantle. The equations above are augmented into a 10 x 10 matrix, A, where where the independent variables are represented in a vector, $\vec{x}$ and the right sides of the equation are represented by the vector $\vec{b}$,

$$\vec{b} = \begin{bmatrix} 0 \\ 0 \\ 0 \\ 0 \\ 0 \\ 0 \\ 0 \\ 0 \\ M_P \end{bmatrix}$$

Thus representing the stoichiometric relationships above in the form $A\vec{x} = \vec{b}$. Now, the independent variables (mole values) may be solved by taking the inverse of A.

$$\begin{aligned} A\vec{x} &= \vec{b} \\ A^{-1}A\vec{x} &= A^{-1}\vec{b} \\ I^2\vec{x} &= A^{-1}\vec{b} \\ \vec{x} &= A^{-1}\vec{b} \end{aligned} \tag{A.21}$$

Where I is the identity matrix. For simplicity and increased computational accuracy, the planet mass is normalized to a value of $M_P = 100$.